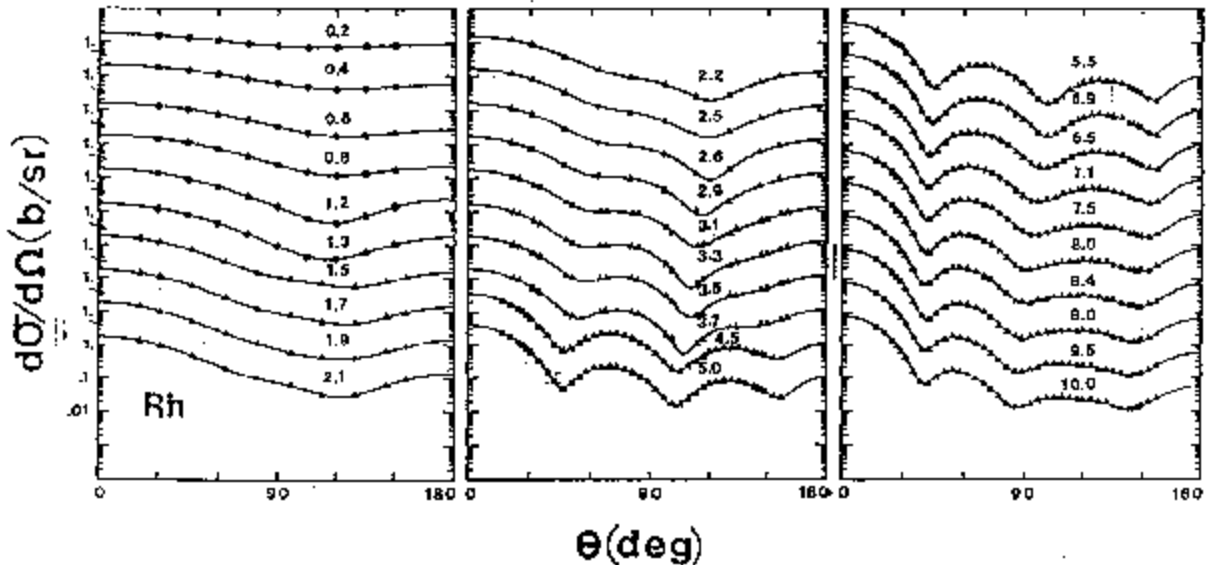


NUCLEAR DATA AND MEASUREMENTS SERIES

ANL/NDM-149
NEUTRONS AND ANTIMONY
PHYSICAL MEASUREMENTS AND INTERPRETATIONS
by
Alan B. Smith
July, 2000



ARGONNE NATIONAL LABORATORY, ARGONNE, ILLINOIS

Operated by THE UNIVERSITY OF CHICAGO

for the U. S. DEPARTMENT OF ENERGY

under Contract W-31-109-Eng-38

ANL/NDM-149
NEUTRONS AND ANTIMONY
PHYSICAL MEASUREMENTS AND INTERPRETATIONS

by
A. B. Smith

Argonne National Laboratory
Argonne, Illinois

July, 2000

Keywords:

Measured $d\sigma/d\Omega_{el}$ and $d\sigma/d\Omega_{inel}$ for 4.5 + 10 MeV neutrons incident on elemental antimony. Comprehensive model interpretations including:- spherical optical-statistical, dispersive and direct-reaction models. Provision of a "general regional" model for applied purposes.

*This work supported by the United States Department of Energy under contract W-31-109-Eng-38, and by the Nuclear and Energy Engineering Program, College of Engineering and Mines, The University of Arizona, Tucson Arizona.

Argonne National Laboratory, with facilities in the states of Illinois and Idaho, is owned by the United States Government, and operated by the University of Chicago under provisions of a contract with the Department of Energy.

Disclaimer

This report was prepared as an account of work sponsored by an agency of the United States Government. Neither the United States Government, nor The University of Chicago, nor any agency thereof, nor any of their employees or officers, makes any warranty, expressed or implied, or assumes any legal liability or responsibility for the accuracy, completeness, or usefulness of any information, apparatus, product, or process disclosed, or represents that its use would not infringe privately owned rights. Reference herein to any specific commercial product, process, or service by trade name, trademark, manufacturer, or otherwise, does not necessarily constitute or imply its endorsement, recommendation, or favoring by the United States Government or any agency thereof. The views and opinions of authors expressed herein do not necessarily state or reflect those of the United States Government or any agency thereof, Argonne National Laboratory, or The University of Chicago.

Available electronically at <http://www.doe.gov/bridge>

Available for a processing fee to U. S. Department of Energy and its contractors, in paper, from:

U. S. Department of Energy
Office of Scientific and Technical Information
P.O. Box 62
Oak Ridge, TN 37831-0062
phone: (865) 576-8401
fax: (865) 576-5728
email: reports@adonis.osti.gov

Nuclear Data and Measurement Series

Reports in the Argonne National Laboratory Nuclear Data and Measurement Series present results of studies in the field of microscopic nuclear data. The primary objective of the series is the dissemination of information in the comprehensive form required for nuclear-technology applications. This Series is devoted to: a) measured microscopic nuclear parameters, b) experimental techniques and facilities employed in measurements, c) the analysis, correlation and interpretation of nuclear data, and d) the compilation and evaluation of nuclear data. Contributions to this Series are reviewed to assure technical competence and, unless otherwise stated, the contents can be formally referenced. This Series does not supplant formal journal publication, but it does provide the more extensive information required for technological applications (e.g., tabulated numerical data) in a timely manner.

PUBLICATIONS IN THE ANL/NDM SERIES

A listing of recent issues in this series is given below. Issues and/or titles prior to ANL/NDM-130 can be obtained from the National Technical Information Service, U. S. Department of Commerce, National Technical Information Service, Technology Administration, Springfield, VA 22161, or by contacting the author of this report at the following address:-

Technology Development Division
Argonne National Laboratory
9700 South Cass Avenue
Argonne, IL 60439
USA

In addition, information on the ANL/NDM Report Series can be found on the Internet at the following URL: <http://www.td.anl.gov/reports/ANLNDMReports.html>. This Internet address contains complete textual and tabular information.

A. B. SMITH AND P. T. GUENTHER

Fast-Neutron Interaction with the Fission Product ^{109}Rh
ANL/NDM-130, September 1993

A. B. SMITH AND P. T. GUENTHER

Fast-Neutron Scattering from Vibrational Palladium Nuclei
ANL/NDM-131, October 1993

A. B. SMITH

Neutron Interaction with Doubly-Magic ^{40}Ca
ANL/NDM-132, December 1993

A. B. SMITH

Neutron Scattering at $Z = 50$: - Tin
ANL/NDM-133, September 1994

A. B. SMITH, S. CHIBA AND J. W. MEADOWS

An Evaluated Neutronic File for Elemental Zirconium
ANL/NDM-134, September 1994

A. B. SMITH

Neutron Scattering from Uranium and Thorium
ANL/NDM-135, February 1995

A. B. SMITH

Neutron Scattering and Models: - Iron
ANL/NDM-136, August 1995

A. B. SMITH

Neutron Scattering and Models: - Silver
ANL/NDM-137, July 1996

A. B. SMITH

Neutron Scattering and Models: - Chromium
ANL/NDM-138, June 1996

W. P. POENITZ AND S. E. AUMEIER

The Simultaneous Evaluation of the Standards and Other Cross Sections of Importance for Technology
ANL/NDM-139, September 1997

- J. T. Daly and D. L. Smith
A Compilation of Information on the $^{31}\text{P}(p,\gamma)^{32}\text{S}$ Reaction and Properties of Excited Levels in ^{32}S
 ANL/NDM-140, November 1997
- A. B. SMITH
Neutron Scattering and Models:- Titanium
 ANL/NDM-141, July 1997
- A. B. SMITH
Neutron Scattering and Models:- Molybdenum
 ANL/NDM-142, July 1999
- R. E. MILLER AND D. L. SMITH
A Compilation of Information on the $^{31}\text{P}(p,\gamma)^{33}\text{Cl}$ Reaction and Properties of Excited Levels in ^{33}Cl
 ANL/NDM-143, July 1997
- R. E. MILLER AND D. L. SMITH
A Compilation of Information on the $^{31}\text{P}(p,\gamma)^{28}\text{Si}$ Reaction and Properties of Excited Levels in ^{28}Si
 ANL/NDM-144, November 1977.
- R. D. LAWSON AND A. B. SMITH
Abarex-A Neutron Spherical Optical-Statistical Model Code: A Users Manual
 ANL/NDM-145, June 1998.
- R. T. KLANN AND W. P. POENITZ
Non-destructive Assay of EBR-II Blanket Elements Using Resonance Transmission Analysis
 ANL/NDM-146, August 1998.
- A. B. SMITH
ELEMENTAL ABAREX -- A User's Manual
 ANL/NDM-147, June 1999.
- D. G. NABEREJNEV AND D. L. SMITH
A Method to Construct Covariance Files in ENDF/B Format for Criticality Safety Applications
 ANL/NDM-148, June 1999.

Table of Contents

Abstract -----	1
1. Introduction -----	1
2. Experimental procedures -----	2
3. Experimental results -----	2
4. Model development -----	4
4-1. Data base -----	4
4-2. Fitting and potential parameters -----	8
i. Simple spherical model (SOM)	
ii. Linear-quadratic model (LQ)	
iii. Quadratic-quadratic model (QQ)	
iv. Strength functions	
v. Core-excitation model (CX)	
5. Physical comments -----	18
5-1. Isospin -----	18
5-2. Dispersive effects -----	19
5-3. Effective mass -----	22
5-4. Quadrupole deformations -----	29
5-5. Shell dependence -----	30
5-6. Comparisons with other potentials -----	30
6. Summary remarks -----	33
Acknowledgments -----	34
References -----	34

NEUTRONS AND ANTIMONY,
PHYSICAL MEASUREMENT AND INTERPRETATIONS

Abstract

New experimental information for the elastic and inelastic scattering of $\approx 4 \rightarrow 10$ MeV neutrons from elemental antimony is presented. The differential measurements are made at ≈ 40 or more scattering angles and at incident neutron-energy intervals of ≈ 0.5 MeV. The present experimental results, those previously reported from this laboratory and as found in the literature are comprehensively interpreted using spherical optical-statistical and dispersive-optical models. Direct vibrational processes via core-excitation, isospin and shell effects are discussed. Antimony models for applications are proposed and compared with "global" "regional" and "specific" models reported in the literature.

1. Introduction

Elemental antimony consists of approximately equal portions of the two isotopes ^{121}Sb and ^{123}Sb . Both of these isotopes are even in neutron number and odd in proton number, with one proton beyond the closed shell at $Z = 50$. In this mass region the extreme shell model indicates very low-energy $1g_{7/2}$ and $2d_{5/2}$ configurations [Law80]. These two single-particle configurations are close together [Coh65, TM69], and the ground and first-excited states shift from $5/2^+$ and $7/2^+$ in ^{121}Sb to $7/2^+$ and $5/2^+$ in ^{123}Sb , respectively. In both cases the first-excited state lies at less than ≈ 0.17 MeV and is generally not resolved in neutron scattering measurements, except at very low incident energies (and has never been resolved in the case of ^{121}Sb). Previous experimental studies of neutron scattering from antimony are largely limited to energies of $\approx < 5$ MeV, and the large majority of the experimental results came from this laboratory ([CC72], [SH67], [SGW82], [SGW84]). Antimony total neutron cross sections are better known but the amount of experimental information above ≈ 15 MeV is sparse (see the total cross section sub-set of the references). Both of these antimony isotopes are minor fission products with cumulative yields of $\approx 10^{-2}\%$ or less [ENDF]. However, they are near the shell closure and at the upper end of the light-mass fission-fragment yield distribution. Thus the fast-neutron interaction with the isotopes of antimony is of applied interest in the context of the systematic behavior of the interaction with light-mass fission products. An objective of this work was the provision of a "regional" optical-statistical model for extrapolation to the neutron

interaction with nearby fission products. At the same time better definition of the fundamental physical nature of the fast-neutron interaction with antimony and its isotopes was sought. ^{121}Sb and ^{123}Sb neutronic evaluated data files are a part of the ENDF/B-6 fission-product evaluated-file system (MAT-5131 and MAT-5125) [ENDF]. Both are largely based upon work more than a quarter century old. The present new experimental results and associated physical understanding make it possible to bring these antimony evaluations up to contemporary standards, as discussed in the companion report, ANL/NDM-150.

2. Experimental procedures

The present measurements were made using the fast time-of-flight method long employed at this laboratory ([CL55],[Smi+92]). Cylindrical measurement samples 2 cm in diameter and 2 cm long of high purity elemental antimony metal were placed ≈ 12 cm from a pulsed neutron source. The source intensity was considerably enhanced by the use of a harmonic bunching system acting on the incident ion beam. The pulse duration was ≈ 1 nsec at a repetition rate of 2 MHz. The neutrons were produced via the $\text{D}(\text{d},\text{n})^3\text{He}$ reaction [Dro87] within a gas target assembly so as to provide neutrons at the scattering sample with an energy spread of ≈ 300 keV at 4.5 MeV, decreasing to ≈ 100 keV at 10.0 MeV. For most of the measurements ten scattered-neutron flight paths of ≈ 5 m length were concurrently used, with scattering angles determined to within $\approx 0.1^\circ$. Some of the higher-resolution inelastic scattering measurements employed ≈ 16 m flight paths and fewer scattering angles (typically three). The scattered-neutron detectors were liquid scintillators, ≈ 12 cm in diameter for the 5 m measurements and ≈ 25 cm in diameter for the 16 m measurements. All cross sections were determined relative to the $\text{H}(\text{n},\text{n})$ standard [CSL83], and all results were corrected for beam-attenuation, multiple-event and angular-resolution effects using monte-carlo techniques [Smi91].

3. Experimental results

The differential elastic-scattering measurements were made at ≈ 0.5 MeV incident-energy intervals from 4.5 + 10.0 MeV and at forty or more scattering angles distributed between $\approx 17^\circ$ and 160° . The effective scattered-neutron resolutions were ≈ 500 keV, thus contributions due to the inelastic-neutron excitation of the first-excited levels in both ^{121}Sb and ^{123}Sb were included with the elastically-scattered component. The implication of this resolution in the interpretation is discussed below. The differential elastic-scattering results are summarized in Fig. 3-1. The normalization uncertainties in these results were estimated to be $\approx 2 + 3\%$, and the statistical uncertainties varied from $\approx 1\%$ to larger quantities in the minima of the

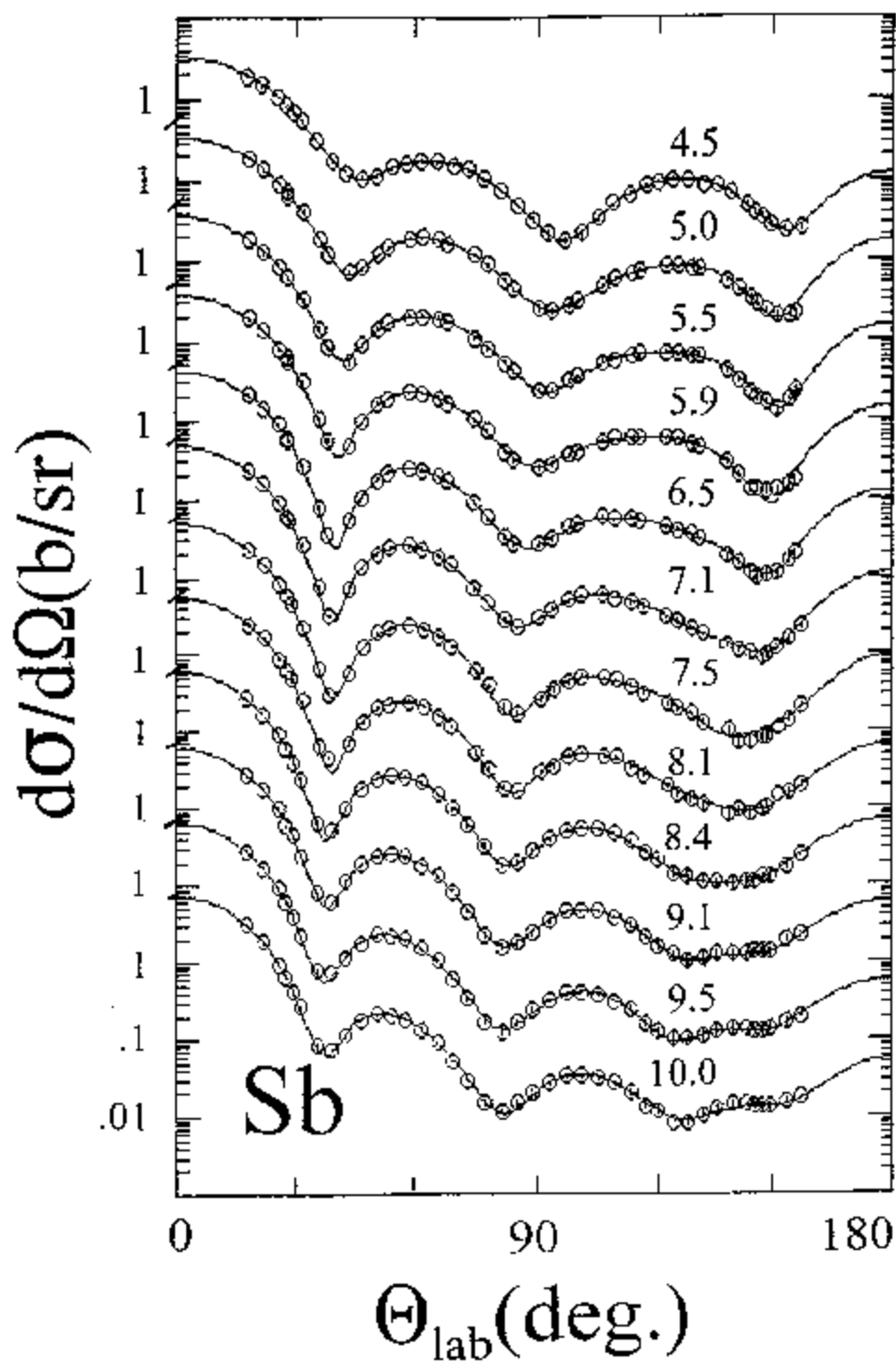


Fig. 3-1. Measured differential "elastic-scattering" cross sections of elemental antimony. Symbols indicate the present experimental results and curves denote legendre fits to the measured values. Numerical values indicate the approximate incident energies in MeV. All figures herein are presented in the laboratory coordinate system.

distributions.

The angular distributions of inelastically-scattered neutrons were measured concurrently with the above elastic-scattering determinations. Contributions from average excitations of ≈ 1.1 , 2.2 and 3.1 MeV were identified. The first of these inelastic groups was by far the best defined, with differential cross sections and their uncertainties illustrated in Fig. 3-2. These cross sections correspond to the cumulative excitation of levels in the excitation-energy range of $\approx 0.5 \rightarrow 1.5$ MeV. As discussed below, there are more than twenty levels in the two isotopes that contribute to these observed cumulative excitations. The resolution of those components transcended the experimental capability. Similar, but less definitive, results were obtained for the excitation of the cumulative levels at ≈ 2.2 and ≈ 3.1 MeV. A few inelastic-scattering measurements were made at $\approx 7 \rightarrow 8$ MeV incident energies and at scattering angles clumped near 80° , using flight paths of ≈ 16 m in order to improve the resolution of the inelastic components. An illustrative time-of-flight spectra obtained at these longer flight paths is shown in Fig. 3-3. Contributions due to levels near 0.55 MeV are resolved with other clumped groups corresponding to excitations of ≈ 1.0 , 1.45, 2.1 and 2.4 MeV, but the experimental resolution remains far from sufficient to fully define the known underlying level structure of the two contributing isotopes. The differential cross sections for the excitation of these inelastic groups are consistent with the lesser resolution results of the above shorter flight-path measurements to within $\approx 20\%$. That is acceptable agreement given the statistical uncertainties and resolution questions in the context of the complex underlying structure.

4. Model Development

4-1. Data Base

The total-cross-section data base was taken from the files of the National Nuclear Data Center and the private files of the Argonne group. The respective components are cited in the total cross section sub-set of the reference list. The experimental total cross section information is not very comprehensive, much of it is very old, and all of the cited values pertain to elemental cross sections. Isotopic antimony total cross sections are limited to several low-energy sets, not relevant to the present considerations, and to a single ≈ 14 MeV measurement [DDK67]. The elemental experimental total cross sections were averaged over 50 keV at incident energies below 0.5 MeV, over 100 keV from 0.5 to 5.0 MeV, and over 200 keV at higher energies in order to smooth fluctuations and reduce the number of data points. The latter energy-averaged values are shown in Fig. 4-1.

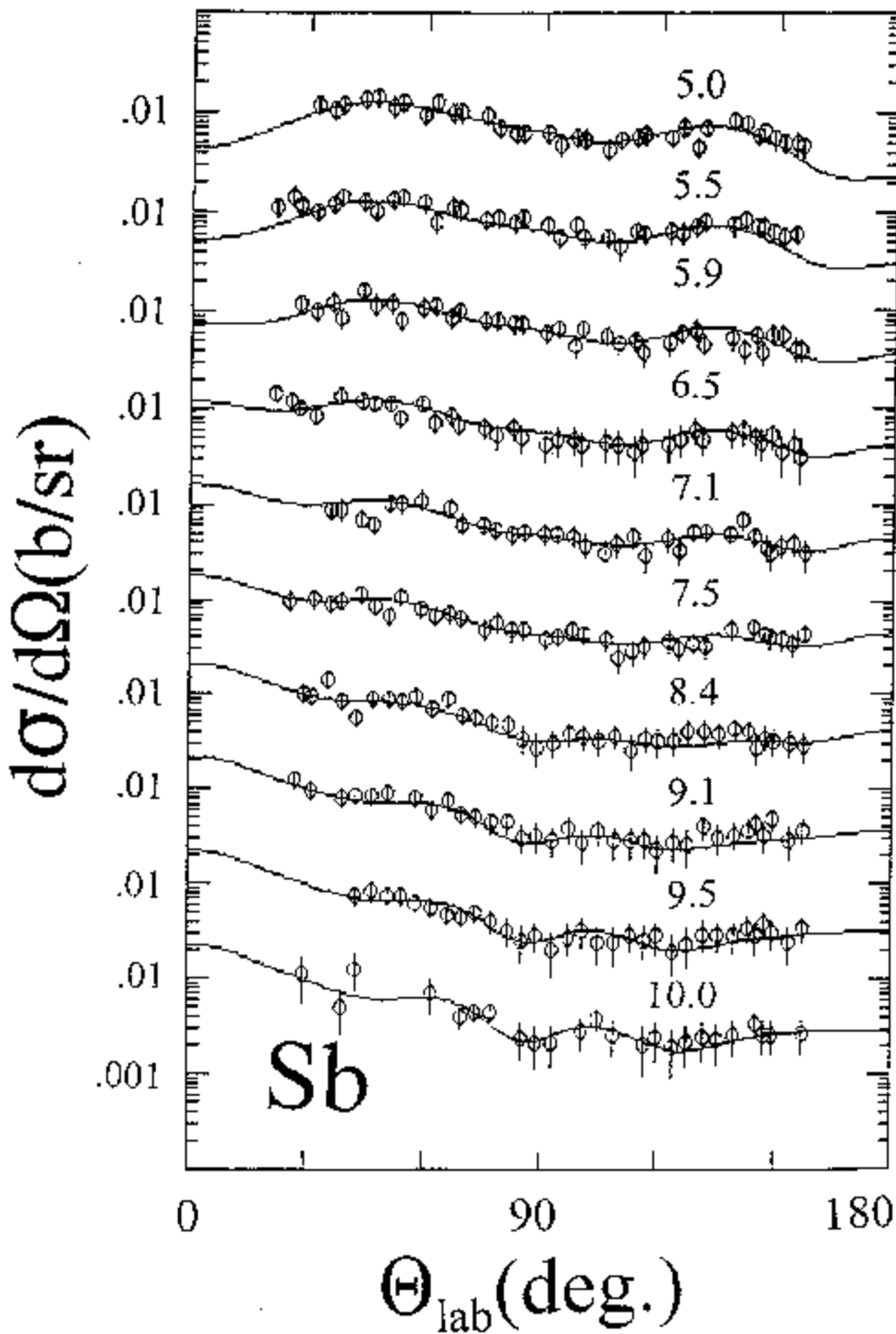


Fig. 3-2. Measured differential "inelastic-scattering" cross sections for the effective excitation of levels in elemental antimony at an energy of ≈ 1.1 MeV. The notation is identical to that of Fig. 3-1, except for the curves which indicate the results of vibrational calculations as described in the text.

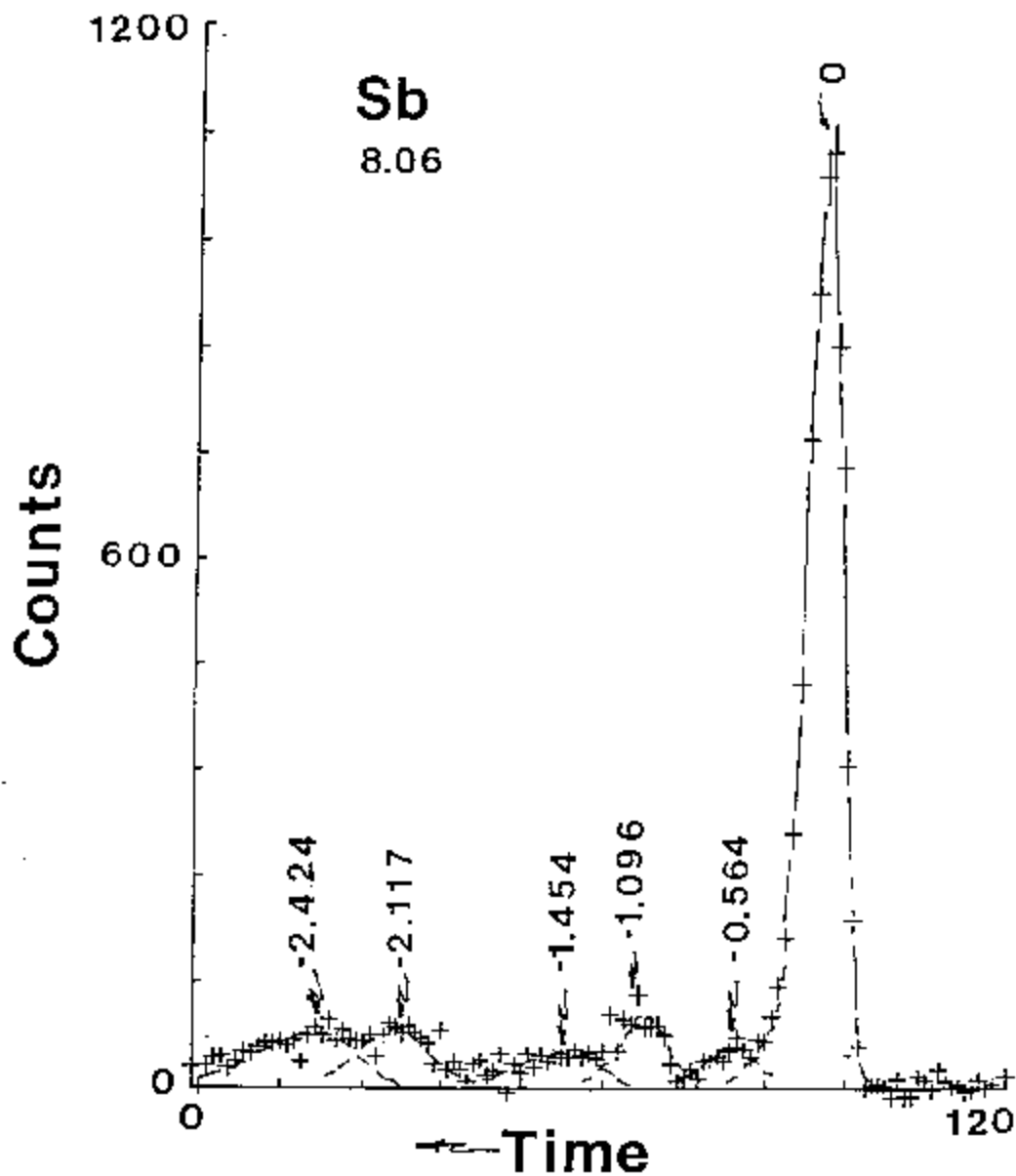


Fig. 3-3. Illustrative time-of-flight spectrum obtained by scattering 8.06 MeV neutrons from elemental antimony over a flight path of ≈ 16 m at an angle of $\approx 80^\circ$. Measured excitation energies of the various peaks are numerically noted in MeV.

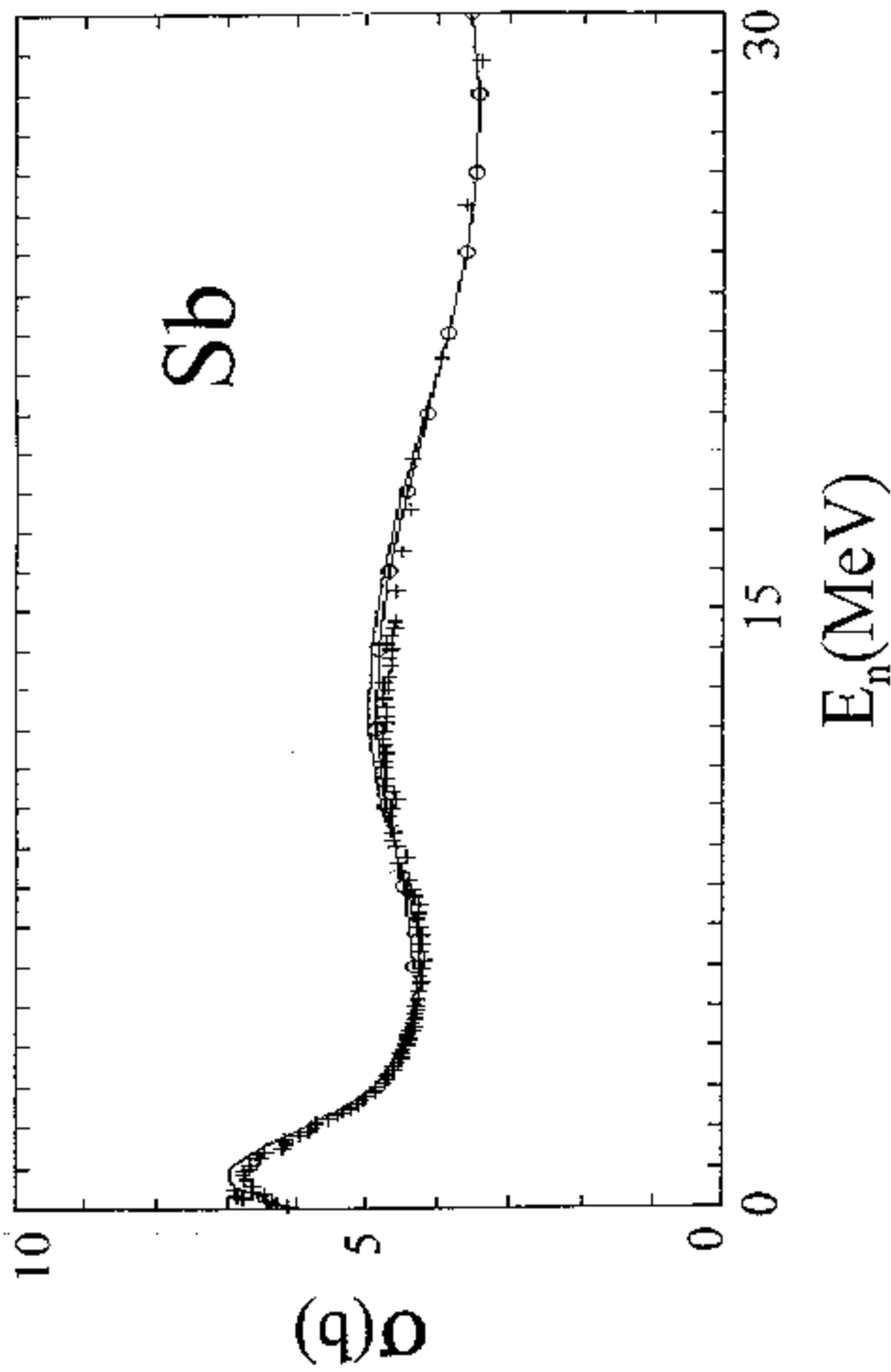


Fig. 4-1. Energy-averaged neutron total cross sections of elemental antimony. The experimental values are indicated by "+" symbols. The simple curve indicates results calculated with the "LQ" model described in the text. The curve with "O" symbols represents the results obtained with the CX model including a direct vibrational interaction, as described in the text.

At the lower energies fluctuations can be a concern in near closed-shell targets such as antimony. Furthermore, they can lead to self-shielding effects that will reduce the observed total cross sections. A few total-cross-section sets in the literature seem to have self-shielding distortions and thus were abandoned.

The elastic-scattering cross sections used in these interpretations were taken from the present work, previous work by the Argonne group, and from the literature. Previously reported work considered in formulating the elastic-scattering data base is cited in the elastic-scattering sub-set of the reference list. Over 90% of the available experimental information comes from the Argonne work. This elastic-scattering data base is illustrated in Fig. 4-2. There are no experimental neutron elastic-scattering results above ≈ 14 MeV (and the 14 MeV distribution is very old), a common shortcoming of neutron studies. The uncertainties assigned to the differential elastic-scattering data were those given by the various workers. In some cases these individuals had considerably different concepts of their uncertainties. Some of the elastic-scattering data sets contained many angular distributions obtained at closely-spaced incident energies, e.g. ref. [SH67]. In those cases the measured values were averaged over ≈ 0.1 MeV incident energy intervals in order to smooth fluctuations and reduce the number of data values to be handled in the interpretations. All of the elastic-scattering results included inelastic-scattering contributions due to the excitation of the first-excited levels of one or both of the two naturally occurring isotopes. Inelastic-scattering data was used in some aspects of the interpretations, as discussed below. That inelastic data is confined to Argonne work of refs. [SH67] and [SGW82], and the present measurements. The large majority of the inelastic-scattering results represent effective cross sections consisting of contributions from several individual components of either isotope.

4-2. Fitting and Potential Parameters

It was assumed that the neutron interaction with elemental antimony could be primarily represented by a spherical optical-statistical model (SOM). Some evidence of direct reactions was dealt with using a coupled-channels model (CCM). The majority of the potential parameters were deduced from fitting procedures minimizing χ^2 defined by

$$\chi^2 = \sum_i \left[\frac{\sigma_{\text{exp}}^{(i)} - \sigma_{\text{cal}}^{(i)}}{\Delta\sigma_{\text{exp}}^{(i)}} \right]^2, \quad (4-1)$$

where $\sigma_{\text{exp}}^{(i)}$ denote measured quantities, $\sigma_{\text{cal}}^{(i)}$ the

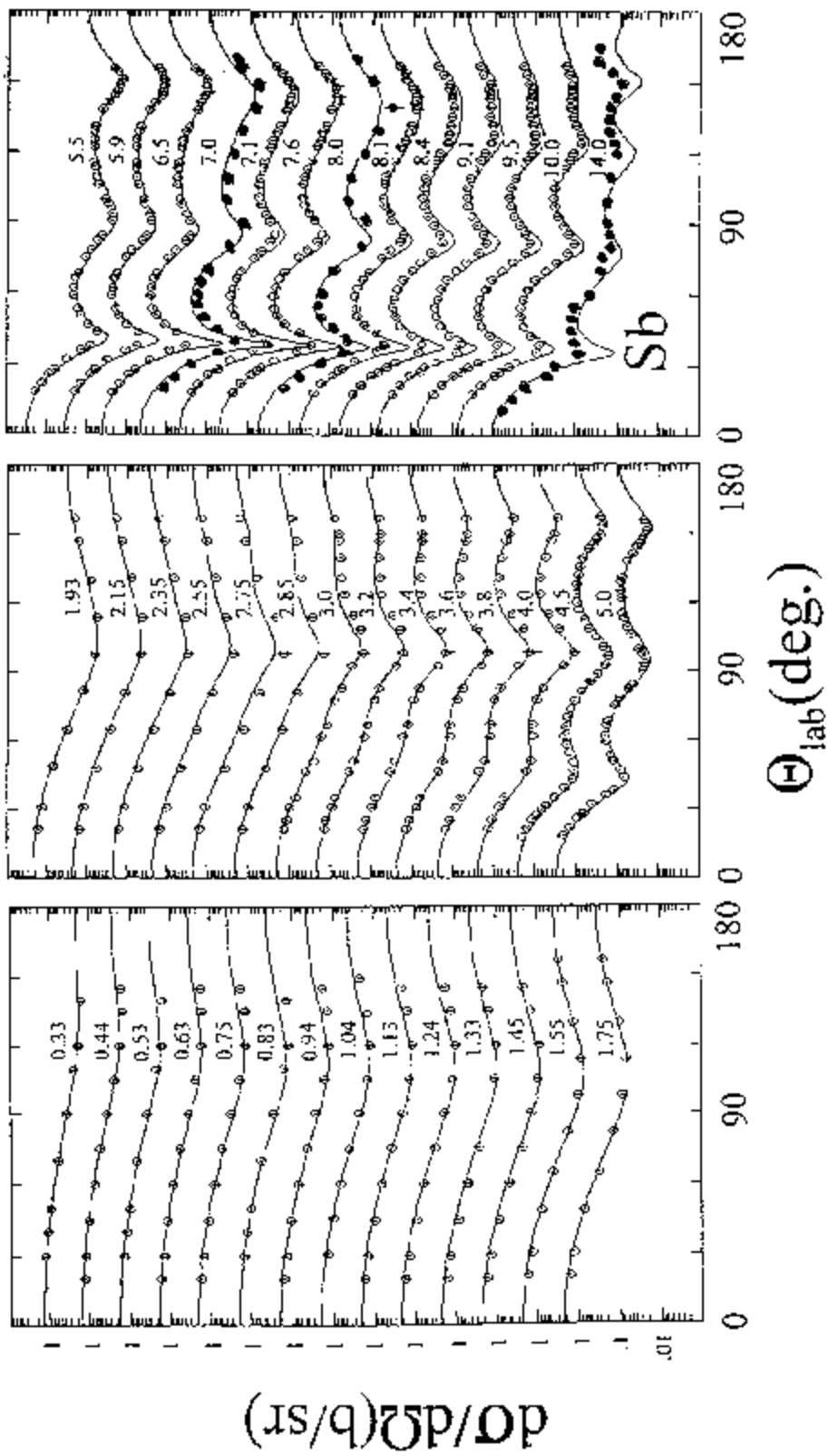


Fig. 4-2. The elastic-scattering data base. Measured values are indicated by circular symbols and curves denote the results of the "LQ" calculations discussed in the text. Approximate incident energies are noted in MeV. More than 90% of the experimental information comes from the present and past work of the Argonne group as noted by open circular symbols. Solid symbols indicate results from other sources as cited in the reference listing.

corresponding calculated values, and $\Delta\sigma_{\text{exp}}$ the measurement uncertainties. All the SOM calculations employed one of the two versions of the computer code ABAREX [Mol82], dealing with isotopic and elemental targets, respectively. All the CCM calculations used the code ECIS96 [Ray96]. Compound-nucleus scattering processes were explicitly dealt with following the formulations of Wolfenstein [Wol51] and Hauser-Feshbach [HF52], as modified for fluctuation and correlation effects by Moldauer [Mol80]. Ten discrete excited states in ^{121}Sb up to excitations of ≈ 1.3 MeV were considered. Their energies, spins and parities were taken from the Nuclear Data Sheets [NDS]. The J^π values of the ground and first excited states of ^{121}Sb are $5/2^+$ and $7/2^+$, respectively. The first-excited state is at ≈ 37 keV and was not experimentally resolved from the elastic scattering in any of the measurements. Thus the calculations included the first-excited inelastic component with the elastic scattering, corresponding to the measurement resolution. The ^{123}Sb calculations were treated in an analogous manner using eleven excited levels up to ≈ 1.5 MeV [NDS], only in this instance the J^π values of the ground and first-excited states are $7/2^+$ and $5/2^+$, respectively, the reverse of the ^{121}Sb case. The inelastic-neutron excitation of the first excited state in ^{123}Sb has been resolved only at low incident energies. The excitation of higher-lying levels was represented using the statistical formalism and parameters of Gilbert and Cameron [GC65]. Neutron radiative capture and other non-scattering neutron-induced reactions were assumed small and ignored.

The real potential was assumed to have the Saxon-Woods form, and the imaginary potential the derivative-Saxon-Woods form [Hod94]. The spin-orbit potential was taken to be real and of the Thomas form with the parameters fixed to those given by Walter and Guss [WG86]. The initial fitting procedures followed the five steps long used by the author [Smi+92]. First, six-parameter fits to the elastic-scattering data base alone were carried out varying real- and imaginary-potential strengths, radii and diffusenesses, from which the real diffuseness, a_v , was fixed. Then, the real radius, r_v , was determined from five-parameter fitting keeping a_v fixed to the above value (herein all radii are expressed in the reduced form where $R_i = r_i \cdot A^{1/3}$ and A is the target mass). Four- and three-parameter fits then progressively determined the imaginary radius, r_w , and imaginary diffuseness, a_w . From this set of successive fitting steps the geometric parameters were determined from the elastic-scattering distributions. This sort of elastic-scattering fitting is sensitive to the partial

angular-momentum components and gives definition of the geometries. At this point the fitting was extended to include total cross sections up to ≈ 30 MeV. The later are sensitive to the total angular momentum but not particularly to the components, however they provide a much wider energy scope for potential determinations than the elastic-scattering alone. Using this elastic-scattering and total cross section data base and the fixed geometry, two-parameter fits determined the real, J_v , and imaginary, J_w , potential strengths expressed in terms of volume-integrals-per-nucleon (J_1).

The initial SOM fitting determining the geometry was confined to elastic scattering and done energy by energy using the above two formulations of ABAREX. In the first of these (termed "el" herein) both isotopes of the element were concurrently fitted assuming real- and imaginary-potential strengths given by $V = V_0 \pm V_1 \cdot \eta$ and $W = W_0 \pm W_1 \cdot \eta$, respectively, where V_0 and W_0 are isoscalar strengths, V_1 and W_1 the isovector strengths and $\eta = (N-Z)/A$, the nuclear asymmetry. The signs in the two expressions are negative for neutron-induced reactions and positive for proton reactions ([Hod71],[Sat69]). The isovector strengths were given the values $V_1 = 24$ MeV and $W_1 = 12$ MeV throughout this work. These magnitudes are generally consistent with average quantities in the literature ([Hod94],[Sat69]). It was further assumed that the form of isoscalar and isovector potentials was the same. The latter assumption is commonly used but is doubtful as V_1 is probably concentrated near the nuclear surface ([Hod94],[Sat69]). However, isovector contributions are relatively small and the two isotopes of antimony have nearly the same η values, therefore this qualitative approximation does not particularly influence the results. In the second approach (termed "iso" herein) the fitting dealt with each isotope separately assuming that the measurements pertained to that isotope alone. A weighted average of the parameters obtained by fitting ^{121}Sb and ^{123}Sb was then constructed to obtain elemental geometric parameter values. The two sets of geometric parameters were very consistent with one another and the average geometric values were used over a large energy range as discussed below.

In an effort to concurrently improve the description of measured elastic-scattering and total cross sections a unified procedure was used in determining real- and imaginary-potential strengths, concurrently fitting the elastic scattering and total cross sections of both isotopes over the entire energy range of available experimental information. Twenty nine experimental elastic distributions were used, extending from 1.55 to 14.0 MeV. Lower-energy distributions were not used as they are "bland" in angular dependence and provide little guidance to the choice of the potential. Thirty one total cross sections, extending from

62 keV to 28 MeV, were constructed from averages of the experimental data base. It was assumed that the real-potential strength had a linear energy dependence. This is consistent with the effects of non-locality and the Hartree-Fock behavior of the potential in a finite medium ([Hod71],[PB62]). The imaginary-potential strength was allowed to take a quadratic energy dependence. This is a reasonable assumption as one would expect the surface-imaginary strength to increase with energy as more channels open and then plateau to an approximately energy-independent value. This model with the linear-quadratic energy-dependent assumptions was termed the "LQ" potential. The potential geometries were fixed to the average of the values resulting from the "el" and "iso" fitting and the isovector strengths were as defined above. The LQ fitting then reduced to the adjustment of five parameters:- (1) the zero-energy intercept value of the isoscalar real potential, (2) its energy dependence, (3) the zero-energy intercept of the isoscalar imaginary potential, (4) its linear and (5) quadratic energy-dependent terms. In concurrently fitting such a data base consisting of total and differential-scattering cross sections judgment must be exercised in the weighting of the input data if both types of data are to effectively contribute to the determination of the model parameters. The two types of data are measured in quite different manners with different types of uncertainties. In the present fitting various relative weights were given to the total cross sections. If each total cross section is given the same weight as each differential value the effect of the total cross sections on the parameter selection is essentially zero. Increasing the weight of each total cross section relative to the differential value, it was found that an enhancement of the weight of the total cross sections by a factor of ≈ 20 , relative to the differential values gave a considerable improvement in the description of the total cross sections over the energy range $0 \rightarrow 30$ MeV while retaining a generally acceptable description of the calculated differential elastic-scattering. The result is compared with the measured elastic-scattering data in Fig. 4-2. The corresponding model parameters are given in Table 4-1. Throughout this work potential parameters are listed to a number of significant figures. This precision makes it possible to accurately reproduce the calculational results, however the significant figures of the stated parameters do not necessarily imply parameter uncertainties. The latter are associated in a complex and uncertain manner with the data bases, the fitting procedures and the weighting factors. The energy dependencies are physically realistic, as discussed below. The agreement between measured and calculated elastic scattering extends to the lower energies of the data base, well below the energies of the distributions used in the parameter derivation. At the same time the description remains good to 10 MeV, with some deterioration at 14 MeV. The latter is a very old (more than 30 years) differential distribution. It would be very useful if there were some good antimony elastic-scattering distributions at higher energies. Concurrently the parameters give a reasonable description of the elemental total cross section to at least 30

Table 4-1. SOM parameters deduced by concurrently fitting differential-elastic and total cross sections of both isotopes. The potentials are given for the "LQ" and "QQ" models, as described in the text. The J_i values are calculated assuming the elemental mass. "E" is the incident energy in MeV and " η " the asymmetry defined as $\eta = (N-Z)/A$.

Real potential

$$a_v = 0.6393 \text{ (fm)}$$

$$r_v = 1.2391 \text{ (fm)}$$

(LQ) model

$$V = 52.5350 - 0.4239 \cdot E - 24.0 \cdot \eta \text{ (MeV)}$$

$$J_v = 463.4 - 3.7391 \cdot E - 211.7 \cdot \eta \text{ (MeV-fm}^3\text{)}$$

(QQ) model

$$V = 52.2598 - 0.1129 \cdot E - 0.0151 \cdot E^2 - 24.0 \cdot \eta \text{ (MeV)}$$

$$J_v = 460.9 - 0.9957 \cdot E - 0.1332 \cdot E^2 - 211.7 \cdot \eta \text{ (MeV-fm}^3\text{)}$$

Imaginary potential

$$a_w = 0.6495 \text{ (fm)}$$

$$r_w = 1.2956 \text{ (fm)}$$

(LQ) model

$$W = 4.7431 + 0.4096 \cdot E - 0.0097 \cdot E^2 - 12.0 \cdot \eta \text{ (MeV)}$$

$$J_w = 54.17 + 4.6780 \cdot E - 0.1108 \cdot E^2 - 137.0 \cdot \eta \text{ (MeV-fm}^3\text{)}$$

(QQ) model

$$W = 4.4000 + 0.4161 \cdot E - 0.0093 \cdot E^2 - 12.0 \cdot \eta \text{ (MeV)}$$

$$J_w = 50.30 + 4.7521 \cdot E - 0.1062 \cdot E^2 - 137.0 \cdot \eta \text{ (MeV-fm}^3\text{)}$$

Spin-orbit potential [WG86]

$$a_{so} = 0.560$$

$$r_{so} = 1.103$$

$$V_{so} = 5.767 - 0.015 \cdot E + 2.0 \cdot \eta \text{ (MeV)}$$

MeV, as illustrated in Fig. 4-1. The measured and calculated values agree to within a few percent over the entire energy range.

Predictably, the total-cross-section description was somewhat improved by assuming a quadratic-quadratic model ("QQ") having quadratic energy dependencies of both the real- and imaginary-potentials, as illustrated in Fig. 4-3, while at the same time providing a somewhat improved description of the elastic scattering, as illustrated in Fig. 4-4. The resulting QQ potential parameters are also given in Table 4-1. The QQ imaginary potential is essentially identical to the LQ result, while the real potential takes a somewhat convex energy dependence that does not greatly differ from the linear LQ shape. The possible contribution of a volume absorption was examined by introducing such a potential in the LQ fitting procedure above 15 MeV. The resulting volume-potential strengths were small with no clear improvement in the description of the observables or the chi-square resulting from the fitting procedures. Volume absorption is doubtless a factor at higher energies but the available antimony experimental data base, largely limited to incident energies below ≈ 10 MeV, does not allow one to identify it.

Both the LQ and QQ potentials are similar as $E \rightarrow 0$ and thus give essentially the same s- and p-wave strength functions (S_0 and S_1 , respectively). The results calculated with the QQ potential are $S_0 = 0.7672$ and $S_1 = 3.235$ for ^{121}Sb and $S_0 = 0.7458$ and $S_1 = 2.926$ for ^{123}Sb (all in units of 10^{-4}). These results are in reasonable agreement with those resulting from other optical-model predictions [MDH81], but the calculated S_0 are approximately a factor of two larger than deduced from experiment. Such S_0 differences are commonly encountered in this mass region and have been attributed to doorway effects [Sha63].

Clearly, the inelastic-scattering results of Fig. 3-2 for an average excitation of ≈ 1.1 MeV are not consistent with the above SOM interpretations. Neither the scattered-neutron angular distributions nor the cross-section magnitudes can be attributed to compound-nucleus processes. There must be significant direct-reaction contributions that make up essentially all of the inelastic-scattering cross sections observed in the present experiments as compound-nucleus contributions are essentially negligible at the energies of the present experiments and the resulting compound inelastically-scattered neutrons should be distributed symmetrically about 90 deg. The antimony isotopes have 51 protons, one beyond the closed shell at 50 protons, and are even in neutron number. Thus, in the context of the extreme

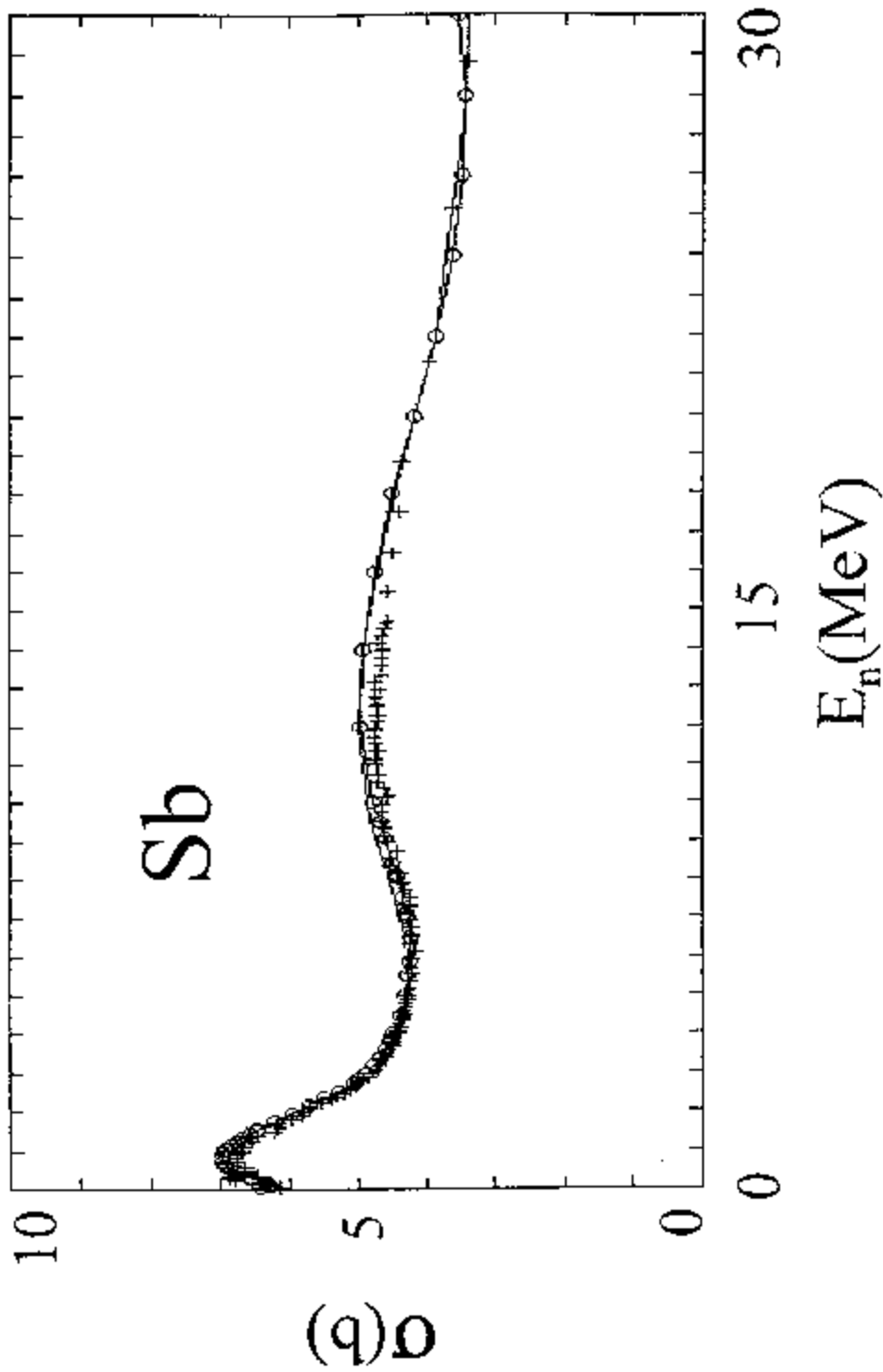


Fig. 4-3. Comparisons of measured and calculated total cross sections. "+" indicate energy-averaged experimental values. The simple curve results from LQ calculations and the curve with circular symbols from QQ calculations, as discussed in the text.

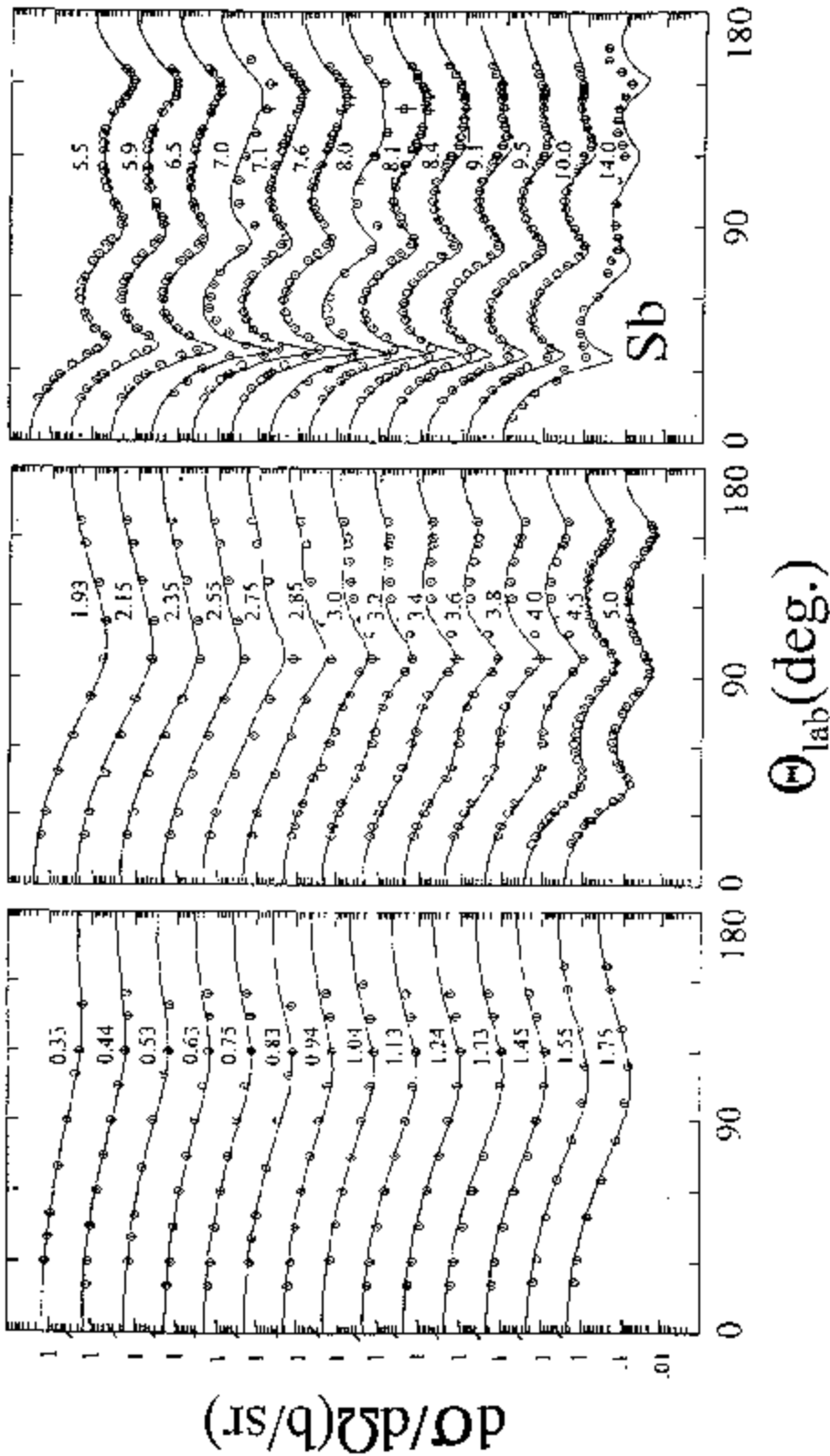


Fig. 4-4. Comparisons of measured and calculated differential elastic-scattering distributions. Circular symbols indicate experimental results and curves the results of QQ model calculations. Numerical values denote the incident energy in MeV.

shell model, the ground and low-lying first excited states can be attributed to the $1g_{7/2}^+$ and $2d_{5/2}^+$ proton configurations, with the $1h_{11/2}^+$ proton configuration lying above ≈ 1.5 MeV [Law80]. The $1g_{7/2}$ and $2d_{5/2}$ configurations are very close together (≈ 100 keV) in this mass region ([Coh65],[TM69]) and, indeed, invert going from ^{121}Sb to ^{123}Sb . The better known structure of ^{123}Sb has ten levels with established spins and parities at excitations from ≈ 0.5 to 1.6 MeV [NDS]. If one assumes that these levels are due to core excitations coupling the $1g_{7/2}$ and $2d_{5/2}$ proton configurations to the $2^+ \approx 1.05$ MeV vibrational level of the ^{122}Sn core, one obtains the ten excited levels reported between ≈ 0.5 and 1.6 MeV, and the assumption is consistent with the reported J^π values. The only exception is a possible additional level at ≈ 1.5 MeV. That level is neither confirmed nor is its J^π value established. Thus, the simple core-excitation approximation is reasonably consistent with the reported ^{123}Sb excited structure that is expected to contribute to the inelastic-scattering resulting in the excitation of the average level in elemental antimony observed at an $E_x \approx 1.1$ MeV in the present experiments. The same simple approximation applies to ^{121}Sb relative to the ^{120}Sn core, although the excited level structure of ^{121}Sb is not as well known. In both cases the direct inelastic scattering could be due to the vibrational nature of the Sn yrast 2^+ levels at ≈ 1.05 MeV. With that assumption, the inelastic-scattering cross sections were calculated using the QQ potential, coupling the g.s. and yrast 2^+ level of the Sn isotopes with a simple first-order vibrational coupling (herein this core-excitation model is termed the "CX model). With a $\beta_2 = 0.115$, the results illustrated by the curves of Fig. 3-2 were obtained. Concurrently, the introduction of the core-coupling contributions improved the description of the measured total cross sections, as illustrated in Fig. 4-1. The agreement between the calculations made with this simple model and the inelastic-scattering values measured in the present work is remarkably good. The inelastic-scattering calculations were not extended to the higher-lying levels due to uncertainties in both the measured structure and its contribution to the observations, but, clearly, direct-reaction mechanisms are again the primary contributors to the inelastic processes observed in the present measurements. There are some measured elemental inelastic-neutron-scattering data for antimony at lower incident energies ([SGW82],[SH67]) where compound-nucleus processes are the dominant factor. In these cases the measured results generally represent averages of complex and uncertain underlying structure. Given these uncertainties, the above SOMs reasonably

account for the lower-energy experimental inelastic-scattering results, as illustrated by the examples given in the companion report, ANL/NDM-150.

5. Physical Comments

5-1. Isospin

It has long been known that the potential strengths are related to isospin through the expression

$$J_i = J_i^0(1 \pm \xi_i \cdot \eta), \quad (5-1)$$

where "+" refers to protons and "-" to neutrons, J_i^0 and ξ_i are constants, η is the asymmetry equal to $(N-Z)/A$, and "i" can be v or w corresponding to the real or imaginary potential, respectively ([Lan62],[GS58]). There are three ways of using neutron-reaction results to determine the constants J_i^0 and ξ_i :-

1) evaluating Eq. 5-1 for a broad isotopic or isobaric range of measurements, 2) comparing (p,p) and (n,n) potential results, and 3) evaluating Eq. 5-1 from potentials over as wide a mass range as possible. The first these methods is not viable in the present study as there are but two isotopes of elemental antimony separated by only two mass units and there are no isotopic or isobaric measurements available. The second method can not be used as relevant (p,p) or other light charged-particle results are little known (none giving detailed potentials). The third method is viable using the SOM potential systematics following from a number of previous studies at this laboratory extending over the wide mass range $\approx 40 \rightarrow 238$ and the asymmetry range $\approx 0 \rightarrow 0.277$ ([Smi96],[Chi+90],[LGS86],[Smi94],[SG93],[Chi+92],[SGL86],[Smi97A],[Smi95],[Smi97],[Smi99],[SC96],[LGS87],[LGS89],[SS97],[SGL88],[Smi+92A]). However, care must be taken to avoid distortions due to common size effects. The reference energy was chosen to be 8 MeV as being central to the range of the data base, an energy not unduly influenced by dispersion effects and an energy reasonably free of compound-nucleus uncertainties. Using this range of potentials, one arrives at the systematic reduced real-potential radius expressed in the form

$$r_v = r_0 + r_1/A^{1/3}, \quad (5-2)$$

where r_0 and r_1 are constants. Least-square fitting to the large data base gives $r_0 = 1.1673$ and $r_1 = 0.37083$ fermis [Smi99]. These values are very similar to the neutron results of ref. [Chi+90] but lead to somewhat smaller r_v values than resulting from some proton studies [Hod70]. For elemental antimony Eq. 5-2

gives $r_v = 1.2421$ fm, compared with the SOM value of 1.2391 deduced in the present work. The agreement between the systematic prediction and the present work is a remarkable 0.2% despite the fact that determinations of r_v by fitting are fraught with the Vr_v^2 ambiguity. The diffusenesses a_v and a_w of Table 4-1 have conventional values. The r_w is significantly greater than the r_v in a manner that is consistent with potentials based upon low-energy strength functions [Mol63]. Thus the geometries of Table 4-1 are supported by a considerable body of previous work.

The systematics of real-potential strengths at 8 MeV are given by

$$J_v = K_0 [1 - \xi_v \cdot \eta] \cdot r_v^3, \quad (5-3)$$

where K_0 and ξ_v are constants [Chi+90]. Again least-square fitting the large potential data base, one obtains $K_0 = 232.96$ MeV-fm³ and $\xi_v = 0.447$ ([Smi99] and references cited therein). Eq. 5-3 predicts at 8 MeV a $J_v = 410.7$ MeV-fm³ for elemental antimony compared with the average of 399.0 MeV-fm³ deduced from the present SOM (LQ). The difference is only $\approx 2.8\%$, a good agreement. Furthermore the ξ_v value is reasonably consistent with that deduced from nucleon-nucleon interactions ([GPT68], [GMP70]), however it is approximately half that obtained from a simple analysis of real potentials across a wide mass range (e.g., [FCR77],[HW72]) as the latter simple approach is distorted by a size effect that approximately doubles ξ_v . One would like to make the same systematic comparisons of J_w values. Unfortunately, J_w is quite sensitive to the nuclear structure of the particular target, resulting in a wide scatter of J_w values.

5-2. Dispersive effects

It is well known that there is a dispersion relationship linking real and imaginary optical potentials and reflecting causality ([Sat83],[Lip66],[Pas67],[Fes58]). This relationship can be expressed in the form

$$J(E)_v = J(E)_{HF} + \frac{P}{\pi} \int_{-\infty}^{+\infty} \frac{J_w(E')}{E - E'} dE', \quad (5-4)$$

where J_{HF} is the strength of the local-equivalent Hartree-Fock potential, J_w is the strength of the imaginary potential, and "P" denotes the principle value of the integral. The integral of Eq. 5-4 can be broken into two parts, a surface component given by ΔJ_s and a volume part given by ΔJ_{vo} , where

$$\Delta J_s = \frac{P}{\pi} \int_{-\infty}^{+\infty} \frac{J_s(E')}{E - E'} dE' \quad (5-5)$$

and

$$\Delta J_{vo} = \frac{P}{\pi} \int_{-\infty}^{+\infty} \frac{J_{vo}(E')}{E - E'} dE'. \quad (5-6)$$

Then $J_v(E) = J_{eff}(E) + \Delta J_s(E)$ and $J_{eff}(E) = J_{HF}(E) + \Delta J_{vo}(E)$, where $J_s(E)$ and $J_{vo}(E)$ are surface and volume imaginary-potential strengths, respectively. J_{HF} and ΔJ_{vo} are approximately linear functions of the energy in the present considerations thus they can not be experimentally distinguished. The effect of Eq. 5-4 is to add a surface component to the real Saxon-Woods potential consisting of some fraction of J_s . The magnitude of this fraction was evaluated using the methods of ref. [LGS87]. It was assumed that the imaginary potential was entirely a surface term up to 25 MeV and then that component fell linearly to zero at 60 MeV. Concurrently, the volume-imaginary potential strength was assumed to increase from zero at 25 MeV to a 60 MeV value equivalent to that of the surface component at 25 MeV. Thus the total imaginary potential strength rose to 25 MeV and then remained constant to higher energies. The J_s was assumed to have a value of zero at the Fermi Energy (E_F), and to follow a quadratic energy dependence from E_F to zero energy, at which point it continued to 25 MeV as given by the LQ model. In addition, the entire imaginary potential was taken to be symmetric about E_F [JLM77]. The Fermi Energies of the two antimony isotopes are similar (-8.024 MeV for ^{121}Sb and -7.718 MeV for ^{123}Sb) and thus a weighted average of $E_F = -7.892$ MeV was used in the dispersive calculations. With these assumptions, the fraction of the surface-imaginary potential added to the the real potential was calculated as a function of energy with the results shown in Fig. 5-1. That fraction falls monotonically with energy from ≈ 0.75 at zero energy to small negative values at 30 MeV. The same calculations give the energy dependence of the above $\Delta J_s(E)$ integral contribution. The latter rises from zero at E_F to $\approx 35 \text{ MeV-fm}^3$ at zero energy and then monotonically falls with

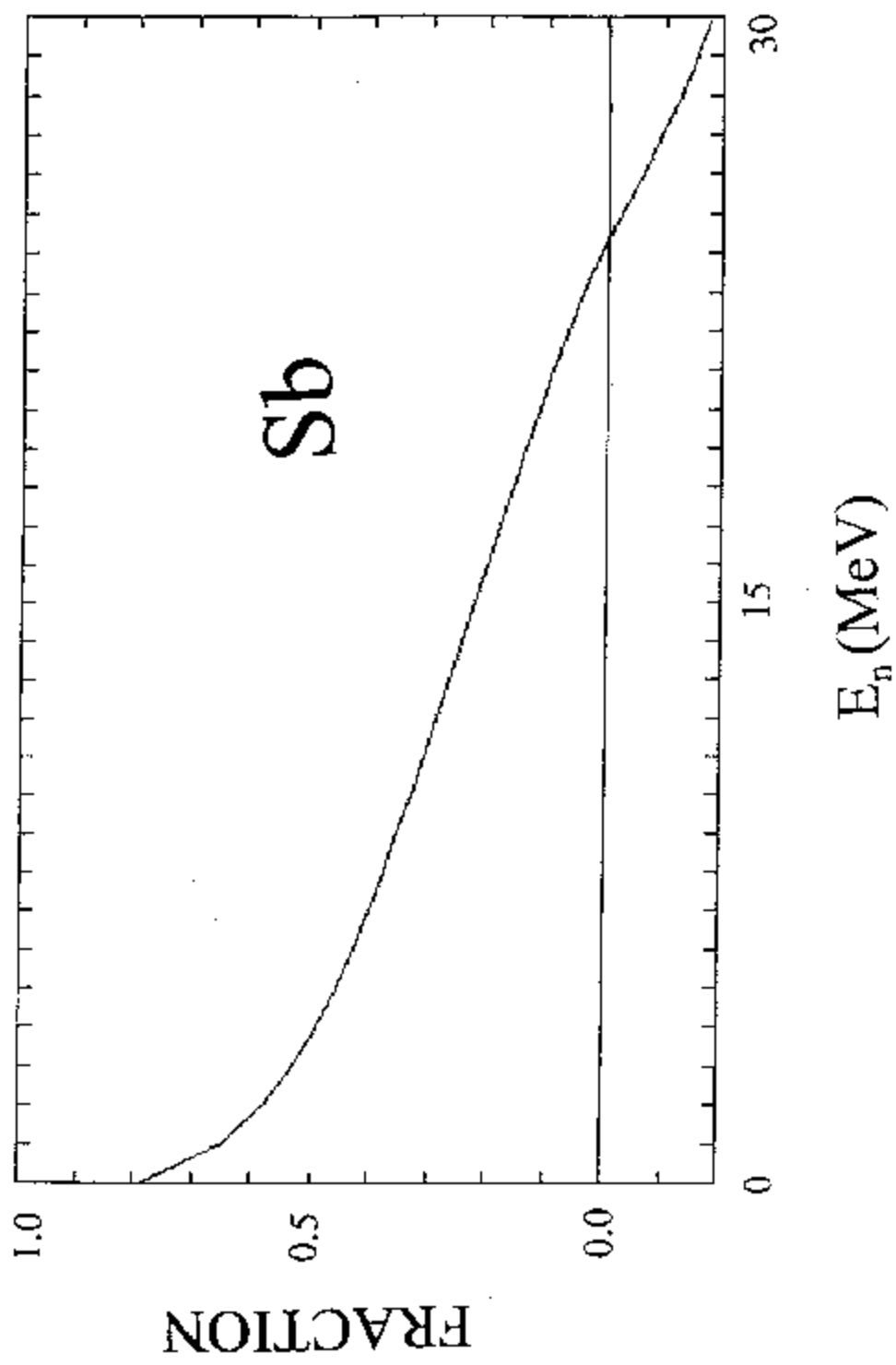


Fig. 5-1. The fraction of the surface-imaginary potential added to the real potential as calculated from Eq. 5-4 of the text.

energy to small values at ≈ 30 MeV as illustrated in Fig. 5-2.

With the above dispersion contribution the entire LQ fitting procedure was repeated. The geometric parameters of the imaginary potential and the real diffuseness were assumed to be the same as those of the LQ model, above. The real-potential radius will change, as the dispersive effect shifts the shape of the real potential, and thus it was a part of the fitting procedure, together with the linear representation of the real potential strength and the quadratic representation of the imaginary strength. The resulting parameters are summarized in Table 5-1 (herein this potential is termed the "Disp-A" potential). In principle the fitting should be iterated to converge on the dispersive effects. This was not done as the potential changes were not large. The results of this fitting procedure gave a very nice description of the experimental total cross sections, as illustrated in Fig. 5-3. However, there was some deterioration of the description of the higher-energy elastic-scattering distributions compared to that of the LQ model results, as illustrated in Fig. 5-4. The characterization of the differential elastic scattering can be improved by increasing the real radius and repeating the fitting procedure employed to determine the parameters of Table 5-1 keeping r_v fixed to the larger value, as illustrated by the parameters of Table 5-2 (herein denoted as the "Disp-AA" model) and the calculated and measured elastic-scattering comparisons of Fig. 5-5. However, this improvement was achieved at the expense of some deterioration of the description of the measured total cross sections. Predictably, these discrepancies can be largely eliminated if all the real- and imaginary-potential geometries are allowed to vary in the fitting procedure. However, the resulting model parameters take rather unphysical values. These considerations suggest that the dispersion effect is significant in the fast-neutron interaction with antimony. However, the experimental data base (particularly with respect to higher-energy elastic scattering) is not sufficiently strong for quantitative assessment of the effect.

5-3. Effective mass

Early on the velocity dependence (i.e. non-locality) of the nuclear potential received considerable attention (e. g., refs. [BLM54],[Bru+56],[Bet56],[PB62] and [WWG60]). It was shown by Brown et al., using a dynamic theory of vibrations, that the non-locality leads to the expression ([BDS79],[MN81],[Bau+82])

$$\frac{m^*}{m} = 0.64 + 0.36[1.0 + |E - E_F|/(2\hbar\omega_0)]^{-2}, \quad (5-7)$$

where "m" is the free nucleon mass, "m*" the effective mass, "E"

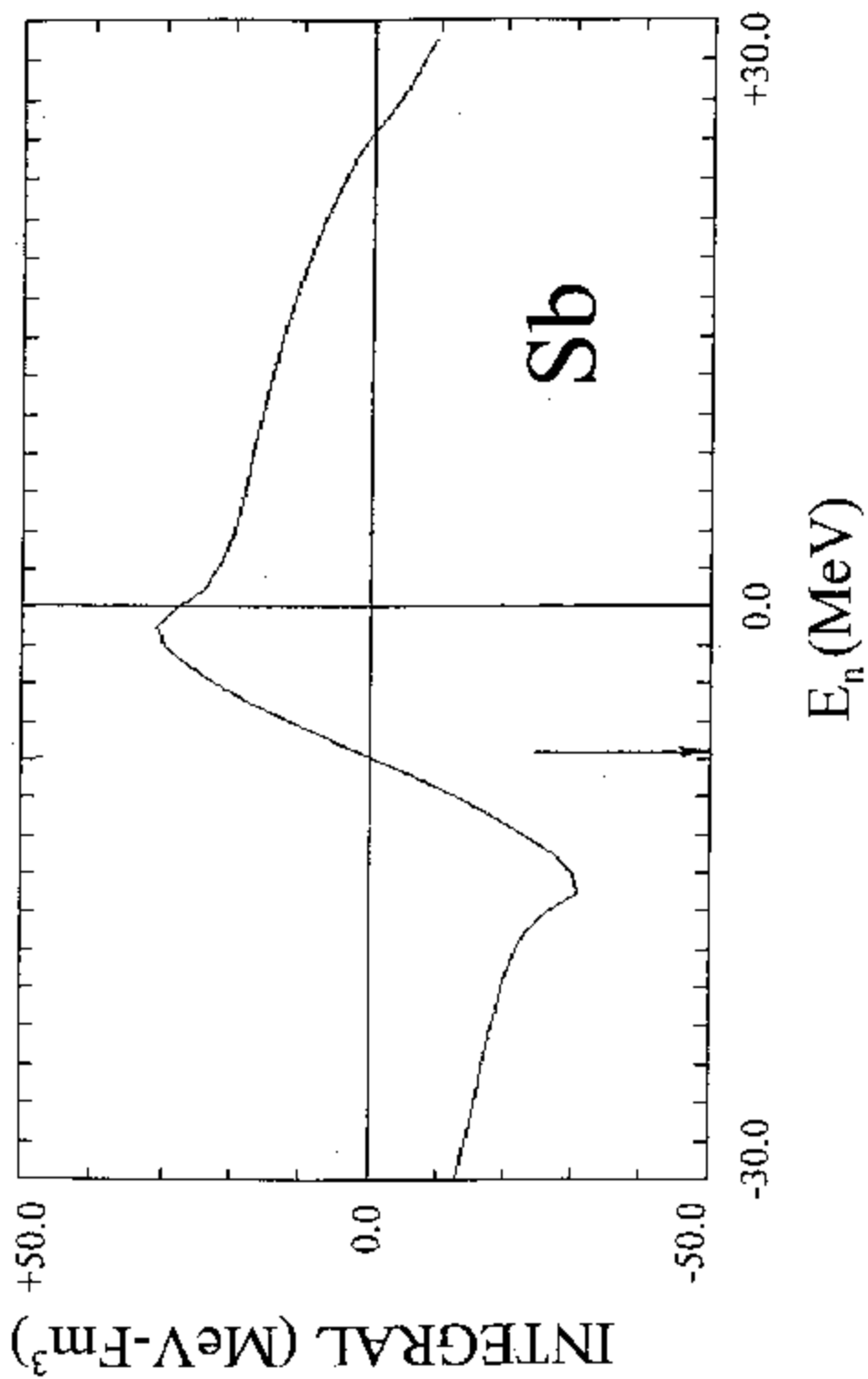


Fig. 5-2. The ΔJ_s integral of Eq. 5-5 calculated as described in the text. The arrow indicates the average Fermi Energy.

Table 5-1. The "Disp-A" model parameters deduced by concurrently fitting differential-elastic and total cross sections of both isotopes, as described in the text. The imaginary-radius, the diffusenesses and the spin-orbit potential are taken from the LQ model of Table 4-2. The J_i values are calculated assuming the elemental mass. "E" is the incident energy in MeV and " η " the average asymmetry defined as $\eta = (N-Z)/A$.

Real potential

$$a_v = 0.6393 \text{ (fm)}$$

$$r_v = 1.1184 \text{ (fm)}$$

$$V = 59.1290 - 0.5248 \cdot E - 24.0 \cdot \eta \text{ (MeV)}$$

$$J_v = 392.0 - 3.4789 \cdot E - 159.1 \cdot \eta \text{ (MeV-fm}^3\text{)}$$

Imaginary potential

$$a_w = 0.6497 \text{ (fm)}$$

$$r_w = 1.2956 \text{ (fm)}$$

$$W = 4.0420 + 0.5669 \cdot E - 0.0121 \cdot E^2 - 12.0 \cdot \eta \text{ (MeV)}$$

$$J_w = 46.2 + 6.4798 \cdot E - 0.1383 \cdot E^2 - 137.2 \cdot \eta \text{ (MeV-fm}^3\text{)}$$

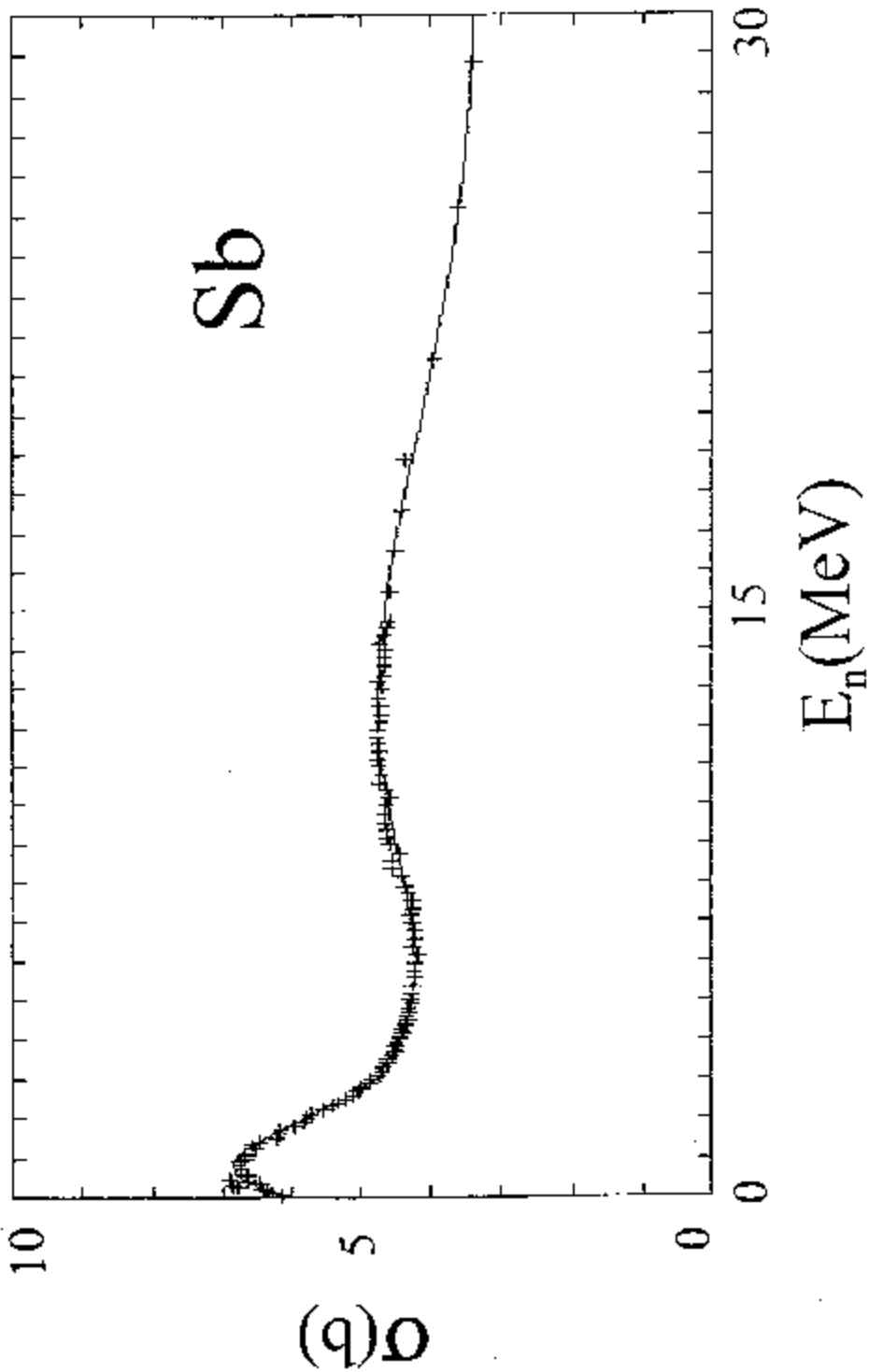


Fig. 5-3. Elemental neutron total cross sections of antimony. Symbols indicate energy-averaged values deduced from the experimental data base as per the text. The curve is the result calculated with the "Disp-A" potential of Table 5-1.

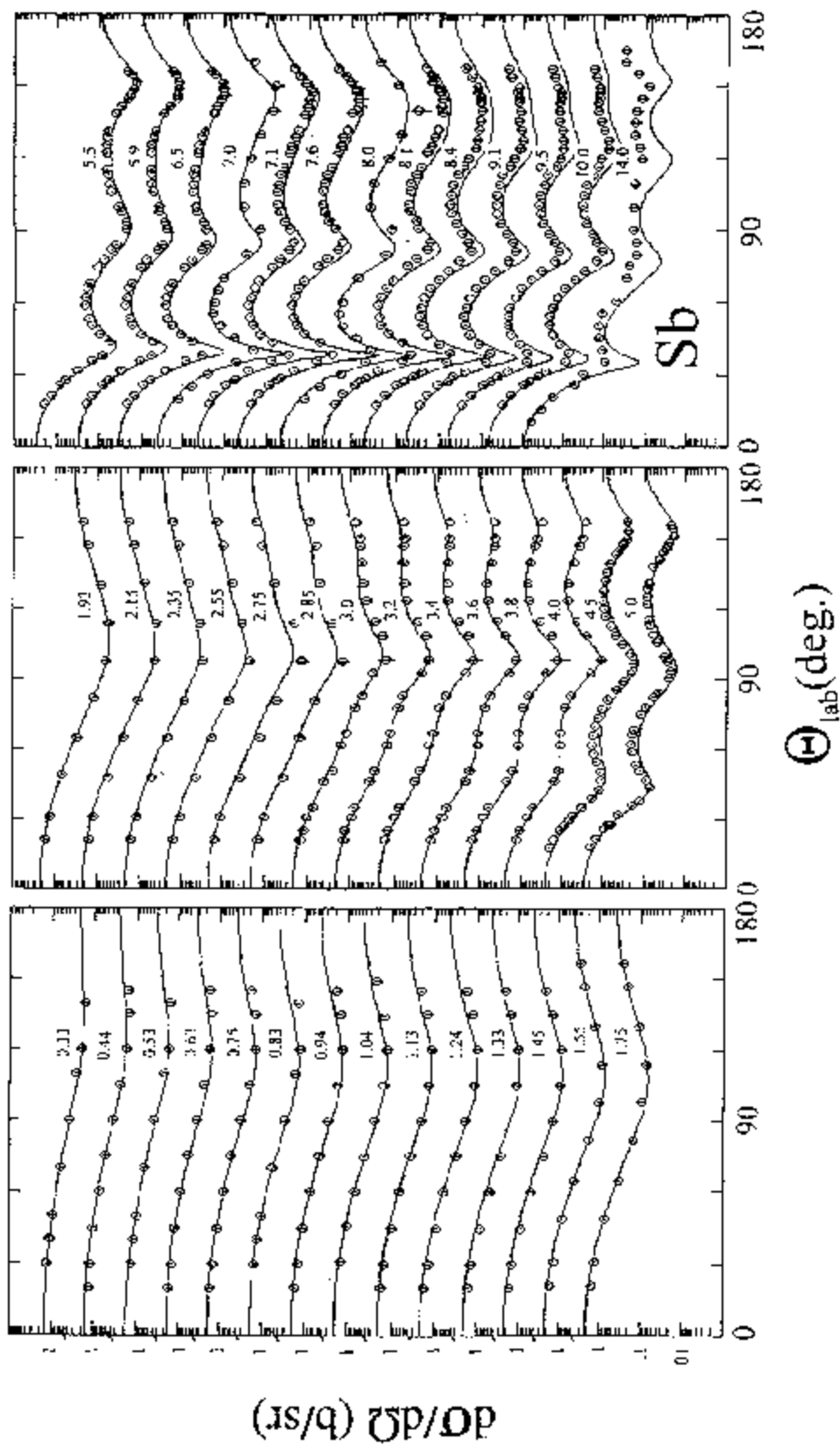


Fig. 5-4. Comparisons of measured and calculated neutron differential elastic scattering. Symbols indicate measured values and curves the results of "Disp-A" model calculations. Incident neutron energies are numerically noted in MeV.

Table 5-2. The "Disp-AA" model parameters deduced by fitting differential-elastic and total cross sections of both isotopes fixing the real-potential radius to 1.2116 and the rest of the geometric parameters to those of Table 5-1, as described in the text. The J_i values are calculated assuming the elemental mass. "E" is the incident energy in MeV and $\eta = (N-Z)/A$.

Real potential

$$a_v = 0.6393 \text{ (fm)}$$

$$r_v = 1.2116 \text{ (fm)}$$

$$V = 52.6581 - 0.3190 \cdot E - 24.0 \cdot \eta \text{ (MeV)}$$

$$J_v = 436.2 - 2.6425 \cdot E - 198.8 \cdot \eta \text{ (MeV-fm}^3\text{)}$$

Imaginary potential

$$a_w = 0.6497 \text{ (fm)}$$

$$r_w = 1.2956 \text{ (fm)}$$

$$W = 4.5036 + 0.2692 \cdot E - 0.0045 \cdot E^2 - 12.0 \cdot \eta \text{ (MeV)}$$

$$J_w = 51.5 + 3.0778 \cdot E - 0.0514 \cdot E^2 - 137.2 \cdot \eta \text{ (MeV-fm}^3\text{)}$$

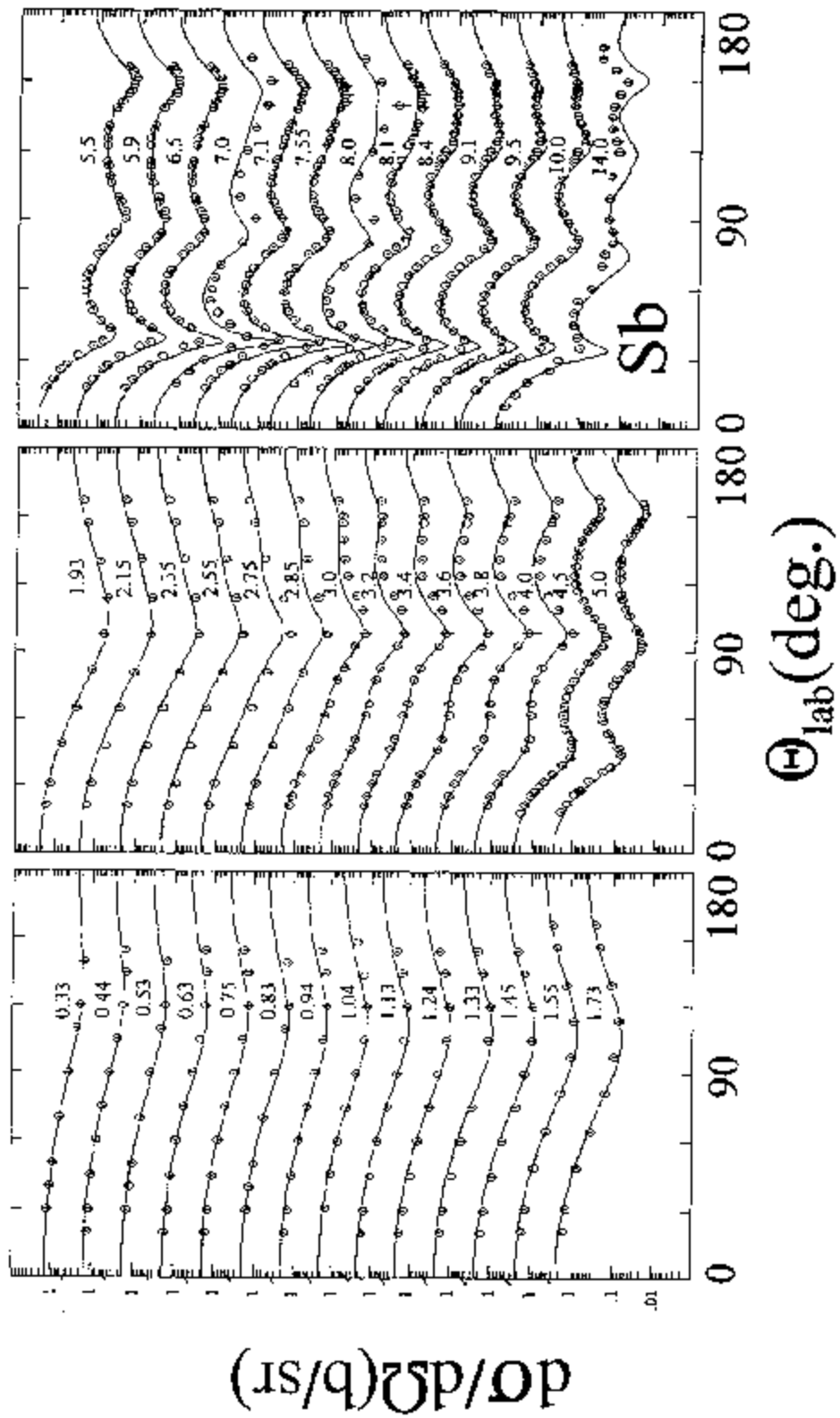


Fig. 5-5. Comparisons of measured and calculated neutron differential elastic scattering. The "Disp-AA" model was used in the calculations. The notation is identical to that of Fig. 5-4.

the energy, " E_F " the Fermi Energy and $\hbar\omega_0 \approx 41/A^{1/3}$. Concurrently,

$$\frac{m^*}{m} = 1 - \frac{dV_L}{dE}, \quad (5-8)$$

where V_L is the local real potential [Sat83]. Well away from E_F , Eq. 5-7 leads to $\frac{m^*}{m} \approx 0.68$, a value consistent with nuclear matter estimates. At E_F , $\frac{m^*}{m}$ of Eq. 5-7 clearly rises to unity which is qualitatively consistent with the shell-model potential in the low-MeV region ([BDS79],[Coh65]). Eq. 5-8 and the present LQ potential imply that $\frac{m^*}{m} \approx 0.58$ well away from E_F . That value is somewhat smaller than indicated by Eq. 5-7 but probably within reasonable uncertainty given the limited range of the data base used in determining the potential.

5-4. Quadrupole deformations

The core-coupling approximation used in the above inelastic-scattering descriptions is based on single proton configurations coupled with the yrast 2^+ levels of the ^{120}Sn and the ^{122}Sn cores. The electro-magnetic quadrupole β_2 values of these two states are 0.1075 and 0.1036, respectively, or an average of ≈ 0.1056 [Ram+87]. The above inelastic-scattering descriptions used a value of $\beta_2 = 0.115$. The tin cores are at closed proton shells thus, in the sense of the core-polarization model of Madsen, Brown and Anderson [MBA75], one should be dealing with neutron vibrators. In such a situation, they predict that the ratio of the β_2^{nn} in the neutron interaction to the β_2^{em} in the electro-magnetic interaction should be $\beta_2^{nn}/\beta_2^{em} \approx 1.063$. The same ratio following from the present inelastic-scattering descriptions is 1.089; a quite good agreement with the theoretical prediction. However, one should more properly compare deformation lengths, conventionally defined by $\delta_2 = \beta_2 \cdot r_v$. Then the ratio following from the present work is $\delta_2^{nn}/\delta_2^{em} \approx 1.125$, still a value reasonably consistent with the theory of ref. [MBA75]. These ratios are encouraging, particularly in view of the approximations used in the present inelastic-scattering descriptions.

5-5. Shell dependence

The isotopes of antimony are only one proton above the closed shell at $Z = 50$. It has been argued by Lane et al. [Lan+59], Brown et al. [BDL59] and others that the absorption strength should be shell dependent with significantly smaller values at or near shell closures. Experimental evidence and the mass dependence of the S_0 strength functions supports such a concept ([VSM64],[MDH81]). The absorption strengths of the present potentials (i. e., "LQ" and "QQ" models) are quite small, particularly at low energies. Not only are these small values consistent with the concept of reduced absorption strengths near shell closures, but they are also in good agreement with the mass dependence of the absorption strength over the mass range $A \approx 90 \rightarrow 125$ as suggested in ref. [SGW84]. In that reference it is shown that absorption strengths are small at or near $N = 50$ and $Z = 50$ closed shells with a pronounced maximum between. This shell modulation of the absorption strength is somewhat distorted by deformation effects but the latter are not a particular concern in the present context. At the higher energies frequently used as a basis for "global" model interpretations shell effects are less prominent and usually ignored. This may be unfortunate as "global" model development tends to place heavy reliance upon closed-shell nuclei such as ^{40}Ca and ^{208}Pb . For example, it is noted below that the "global" model of ref. [RKF79], largely based upon closed-shell nuclides, has an unusually small absorption strength. Shell-dependent absorption effects are not unique to neutron processes, and have been observed in a variety of charge-particle reactions (e.g., [JGK79],[Her+80] and [FHG82]). Models should be cognizant of the shell dependence of the absorption strength if the objective is quantitative calculation. Failure to do so may have been a contributing factor in the deterioration of antimony results calculated with several "global" models, as discussed below. Some "regional" models giving attention to shell effects (e.g., that of ref. [SGW84]) do much better.

5-6. Comparisons with Other Potentials

It is of interest to compare the present potentials with a sampling of spherical potentials found in the literature. Such comparisons can give guidance in the use of models for the provision of antimony data for applied purposes, and can illuminate some physical differences. There are a great number of optical-model potentials found in the literature, of variable qualities and physical scope. Here the comparisons are limited to a few of the more prominent reported "global" potentials, and to a specific antimony potential.

The first comparison is with the SGW "specific" potential (Smith, Guenther and Whalen, ref. [SGW82]). The SGW potential was deduced from elemental antimony low-energy (i.e., $< 4\text{-}5$ MeV) neutron total and elastic-scattering data. It is a simple

potential with strengths $J_v = 429.9 - 2.667 \cdot E \text{ MeV-fm}^3$ and $J_w(\text{surface}) = 54.0 \text{ MeV-fm}^3$. These strengths are reasonably consistent with those of the present "LQ" and "QQ" potentials. The SGW gives as good a description of the elemental elastic-scattering distributions and total cross sections as obtained with the present LQ and QQ potentials. This good performance of the SGW potential is surprising as it was determined only from low-energy experimental information and yet it nicely extrapolates upward in energy by nearly an order of magnitude. For many applications the simple SGW potential will suffice, and it is easy to use.

The second comparison is with the BG "global" potential (Becchetti and Greenlees, ref. [BG69]). This is a widely referenced potential that is largely based upon proton data. It should be generally applicable to antimony in the range of the present studies. The strengths of this potential for the neutron interaction with antimony are $J_v = 409.5 - 2.501 \cdot E \text{ MeV-fm}^3$ and $J_w(\text{surface}) = 106.1 - 2.402 \cdot E \text{ MeV-fm}^3$. In addition, there is volume absorption above an incident energy of $\approx 7 \text{ MeV}$. The J_v of the BG potential is smaller than that implied by the present work, though the difference is partly compensated for by a lesser energy dependence. The imaginary strength is larger than indicated by the present work and has an unusual energy dependence. One would have thought that the surface-imaginary strength would increase with energy up to ten or more MeV as more channels open, contrary to the behavior of the BG potential. The BG potential leads to antimony elastic-scattering angular distributions above $\approx 5 \text{ MeV}$ that are not representative of the measured values. The antimony total cross sections calculated with the BG potential differ from the measured values by $\pm 5\text{-}10\%$ below $\approx 15 \text{ MeV}$, depending upon where the comparisons are made.

The WH "global" potential (Wilmore and Hodgson, ref. [WH64]) is an early and simple potential that contains no spin-orbit interaction. The potential strengths are $J_v = 451.5 - 2.564 \cdot E - 0.0173 \cdot E^2 \text{ MeV-fm}^3$ and $J_w(\text{surface}) = 73.1 - 0.407 \cdot E \text{ MeV-fm}^3$. The J_v for antimony is larger than found in the present work and the energy dependence of the J_w is hard to justify, as noted above. The elastic-scattering distributions calculated with the WH potential significantly deviate from the measured values above $\approx 4 \text{ MeV}$, particularly at large angles. The calculated total cross sections agree reasonably well with the measured values above $\approx 15 \text{ MeV}$ but at lower energies there are significant differences, both positive and negative. Thus the WH potential is not suggested for quantitative antimony calculations in the energy

range of the present considerations.

The WG "global" potential (Walter and Guss, ref. [WG86]) is based upon both neutron and proton experimental data (including neutron polarizations). The strengths are $J_v = 426.8 - 2.540 \cdot E$ MeV-fm³ and $J_w(\text{surface}) = 73.4 - 1.368 \cdot E$ MeV-fm³. The former is reasonably consistent with that of the present work, but the latter again shows a negative energy dependence very likely resulting from the higher energies used in developing the model. Concurrently, there is a significant volume-absorption strength at all energies, an unusual configuration that is not supported by the present interpretations. The WG potential does not give a good description of the antimony elastic-scattering distributions above ≈ 3.5 MeV and is significantly discrepant with the measured total cross sections (both positive and negative deviations) below ≈ 15 MeV.

The RKF "global" model (Rapaport, Kulkarni and Finlay, ref. [RKF79]) was deduced from neutron interactions with closed-shell targets for incident neutron energies of $\approx 7 - 26$ MeV. Antimony is near a closed shell so this potential should be reasonably applicable in the present context. The strengths are $J_v = 408.4 - 2.418 \cdot E$ MeV-fm³ and $J_w(\text{surface}) = 22.6 + 4.12 \cdot E$ MeV-fm³ for $E \leq 15$ MeV. There is another branch of J_w for $E > 15$ MeV that seems to be significantly discontinuous with the lower energy branch. There is also an increasing volume absorption term above 15 MeV. The J_v is lower than found in the present work though the difference is partly compensated for by a lesser energy dependence. The imaginary strength has a strong energy dependence and is very small at low energies. The antimony elastic scattering calculated with the RKF potential is in good agreement with the observations, approximately equivalent to the descriptions obtained with the LQ model, above. The description of the antimony total cross sections is good above about ≈ 10 MeV but deteriorates at lower energies, with discrepancies of $\pm 5-10\%$ from the measured values. However, of the "global" models examined here, the RKF potential provided the best antimony results.

The EF "global" potential (Engelbrecht and Fiedeldey, ref. [EF67]) is an extension of the low-energy model of Moldauer [Mol63] to higher energies using complicated exponential energy dependencies of the real and imaginary strengths. The higher-energy considerations extend to 150 MeV. The parameterization is awkward and no conventional spherical optical model code that will handle it is known to the author. The comparisons made here required some modification of the ABAREX calculational code. The antimony elastic-scattering calculated with the EF potential is in qualitative agreement with measured values but with quantitative discrepancies above ≈ 5

MeV. The agreement between calculated and measured total cross sections is good above ≈ 13 MeV but at lower energies there are significant discrepancies, with the calculated results generally lying low. The performance of the EF potential in the antimony calculations is not outstanding.

The above non-inclusive comparisons indicate that SGW and RKF potentials give reasonable descriptions of the measured antimony neutron-interactions. These descriptions are not quite as good as obtained in the detailed studies of this work. The other potentials examined (BG, WH, WG and EF) have serious shortcomings that make them questionable for quantitative calculations in the present context. There are many other optical-model potentials out in the literature [PP76]. None of them is unique and very possibly there are others beyond those examined here that would give suitable or better antimony results. However, if the practitioner wants quantitative results one should be very careful in the selection of the potentials used. Of course, one would expect "specific" or "regional" potentials to perform better than "global" potentials as they should reflect individual structural effects of the particular targets.

6. Summary Remarks

The present measurements considerably extend the experimental knowledge of fast-neutron scattering from elemental antimony. That understanding is now reasonably good up to ≈ 10 MeV, but essentially nothing is known at higher energies nor with respect to isotopic antimony neutron scattering. These remaining deficiencies inhibit both basic and applied understanding.

Spherical optical potentials were deduced from the available neutron total and scattering information using both linear and quadratic energy dependencies of the potential strengths. These models were reasonably descriptive of the observables, including neutron total and elastic-scattering cross sections. They also provided S_0 and S_1 strength functions similar to those obtained with other optical potentials found in the literature. However, the S_0 values are not as small as reported by some measurements, possibly as a consequence of specific structural effects not consistent with the model. The inelastic neutron scattering observed in the present measurements is inconsistent with compound-nucleus concepts and thus is largely, if not completely, due to direct-scattering processes. It is well described by a simple core-coupling model coupling the the yrast $5/2^+$ and $7/2^+$ levels of the two antimony isotopes to the yrast 2^+ quadrupole vibrational levels at ≈ 1.1 MeV of the underlying ^{120}Sn and ^{122}Sn closed-shell cores. The quadrupole deformations used in the inelastic calculations are reasonably consistent with those deduced from coulomb excitation studies and with the prediction

of the core-coupling model.

The present antimony interpretations are consistent with systematics of real-potential geometry and strengths as deduced from specific potentials generated as a result of a large number of Argonne studies. The resulting isospin dependence agrees with that deduced from the consideration of nucleon-nucleon forces. Dispersive effects are an important consideration with significant impact on the calculated total and scattering cross sections. Unfortunately, the lack of a higher-energy data base for interpretation compromises the quantitative analysis of the dispersive processes. The present potentials imply an effective mass that is qualitatively consistent with theoretical estimates and single-particle configurations. The present potentials are characterized by relatively small imaginary-potential strengths as one would expect for targets near the closed shell at $Z = 50$.

The antimony SOM potentials deduced in the present work are a good vehicle for applied antimony calculations. They provide calculated results notably better than most global and regional models. Such an application of these models to the provision of comprehensive neutronic evaluated files for ^{121}Sb and ^{123}Sb in the ENDF-6 formats is described in the companion report, ANL/NDM-150. The reader is encouraged to examine that document. It is a good illustration of the application of the present work, and presents a number of additional comparisons of measured and calculated quantities in a wide scope.

Acknowledgments

The author is very much indebted to the staff of the National Nuclear Data Center, Brookhaven National Laboratory, for the provision of a large amount of measured data from their files. He also very much acknowledges the hospitality of the Technology Development Division, Argonne National Laboratory. Without their continued tolerance this work would have been impossible.

References:-

1. General

- [Bau+82] Bauer M., Hernandez-Saldana E., Hodgson P. and Quintanilla J., J. Phys. G8 (1982) 525.
- [BDS79] Brown G., Debesa J. and Speth J., Nucl. Phys. A330 (1979) 290.
- [Bet56] Bethe H., Phys. Rev. 103 (1956) 1353.
- [BG69] Becchetti F. Jr. and Greenlees G., Phys. Rev. 182 (1969) 1190.
- [BLM54] Brueckner K., Levinson C. and Mahmoud H., Phys. Rev. 95 (1954) 217.

- [BDL59] Brown G., DeDominicus C. and Langer J., *Ann. Phys.* **6** (1959) 209.
- [Bru+56] Brueckner K., *Phys. Rev.* **103** (1956) 1121.
- [CC72] Cox S. and Cox E., Argonne National Laboratory Report ANL-7935 (1972).
- [Chi+90] Chiba S., Guenther P., Lawson R. and Smith A., *Phys. Rev.* **C42** (1990) 2487.
- [Chi+92] Chiba S., Guenther P., Smith A., Sugimoto M. and Lawson R., *Phys. Rev.* **C45** (1992) 1260.
- [Coh65] Cohen B., *Am. J. Phys.* **33** (1965) 1011.
- [CL55] Cranberg L. and Levin J., *Proc. Conf. on Peaceful Uses of Atomic Energy, Geneva* (United Nations Press, New York, 1955)
- [CSL83] Nuclear Standards File, IAEA Tech. Report 227, eds. Conde H., Smith A. and Lorenz A. (1983); and the ENDF/B-6 nuclear standards file.
- [Dro87] Drosz M., IAEA Report, IAEA-TECDOC-410 (1987).
- [DDK67] Dukarevich J., Djumin A. and Kaminker D., *Nucl. Phys.* **A92** (1967) 433.
- [EF67] Engelbrecht C. and Fiedeldej H., *Ann. Phys.* **42** (1967) 262.
- [ENDF] Evaluated Nuclear Data File/B version 6, available from the National Nuclear Data Center, Brookhaven National Laboratory.
- [FCR77] Ferrer J., Carlson J. and Rapaport J., *Nucl. Phys.* **A275** (1977) 325.
- [Fes58] Feshbach H., *Ann. Rev. Nucl. Sci.* **8** (1958) 49.
- [FHG82] Flynn D., Hershberger R. and Gabbard F., *Phys. Rev.* **C26** (1982) 1744.
- [GC65] Gilbert A. and Cameron A., *Can. J. Phys.* **43** (1965) 1446.
- [GMP70] Greenlees W., Makifske W. and Pyle G., *Phys. Rev.* **C1** (1970) 1145.
- [GPT68] Greenlees W., Pyle G. and Tang Y., *Phys. Rev.* **171** (1968) 1115.
- [GS58] Green A. and Sood P., *Phys. Rev.* **111** (1958) 1147.
- [Her+80] Hershberger R., Flynn D., Gabbard F. and Johnson C., *Phys. Rev.* **C21** (1980) 896.
- [HF52] Hauser W. and Feshbach H., *Phys. Rev.* **87** (1952) 362.
- [Hod70] Hodgson P., *Nucl. Phys.* **A150** (1970) 1.
- [Hod71] Hodgson P. E., Nuclear reactions and nuclear structure (Clarendon, Oxford, 1971).
- [Hod94] Hodgson P. E., The nucleon optical model (World Scientific, Singapore, 1994).
- [HW72] Holmqvist T. and Wiedling T., *Nucl. Phys.* **A188** (1972) 24.
- [JLM77] Jeukenne J., Lejeune A. and Mahaux C., *Phys. Rev.* **C16** (1977) 80.
- [JGK79] Johnson C., Galonsky A. and Kernell R., *Phys. Rev.* **C20** (1979) 2052.
- [Lan+59] Lane A., Lynn J., Melkonian E. and Rae E., *Phys. Rev. Lett.* **2** (1959) 424.
- [Lan62] Lane A., *Nucl. Phys.* **35** (1962) 676; also *Phys. Rev. Lett.* **8** (1962) 171.

- [Law80] Lawson R. D., The theory of the nuclear shell model (Clarendon, Oxford, 1980).
- [LGS86] Lawson R., Guenther P. and Smith A., Phys. Rev. C34 (1986) 1599.
- [LGS87] Lawson R., Guenther P. and Smith A., Phys. Rev. C36 (1987) 1298.
- [LGS89] Lawson R., Guenther P. and Smith A., Nucl. Phys. A493 (1989) 267.
- [Lip66] Lipperheide R., Nucl. Phys. 89 (1966) 97.
- [MBA75] Madsen V., Brown V. and Anderson J., Phys. Rev. C12 (1975) 1205.
- [MDH81] Mughabghab S., Divadeenam M. and Holden N., Neutron cross sections (Academic, New York, 1981).
- [MN81] Mahaux C. and Ngo H., Phys. Lett. B100 (1981) 285.
- [Mol63] Moldauer P., Nucl. Phys. 47 (1963) 65.
- [Mol80] Moldauer P., Nucl. Phys. A344 (1980) 185.
- [Mol82] Moldauer P., Spherical Optical-Statistical Model Code ABAREX, private communication (1982); Extensively modified by Lawson R., Smith A. and Chiba S. as described in the Argonne National Laboratory Reports ANL/NDM-145 (1998) and ANL/NDM-147 (1999).
- [NDS] Tamura T., Iimura H., Miyano K. and Ohya S., Nucl. Data Sheets 64 (1991) 323; also Ohya S. and Tamura T., Nucl. Data Sheets 70 (1993) 53.
- [Pas67] Passatore G., Nucl. Phys. A95 (1967).
- [PB62] Perey F. and Buck B., Nucl. Phys. 32 (1962) 353.
- [PP76] Perey C. and Perey F., At. Data and Nucl. Data Tables 17 (1976) 1.
- [Ram+87] Raman S., Malarkey C. Millet W., Nestor C. Jr. and Stelson P., At. Data and Nucl. Data Tables 36 (1987) 1.
- [Ray96] Raynal J., The Coupled-Channels Code ECIS96, private communication (1996); see also the CEA Report CEA-N-2772 (1994).
- [RKF79] Rapaport J., Kulkarni V. and Finlay R., Nucl. Phys. A330 (1979) 15.
- [Sat69] Satchler G., Isospin in nuclear physics Ed. D. Wilkinson (North-Holland, Amsterdam, 1969).
- [Sat83] Satchler G., Direct nuclear reactions (Clarendon, Oxford, 1983).
- [SC96] Smith A. and Chiba S., Ann. Nucl. En. 23 (1996) 459.
- [SG93] Smith A. and Guenther P., J. Phys. G19 (1993) 655.
- [SGL86] Smith A., Guenther P. and Lawson R., Nucl. Phys. A455 (1986) 344.
- [SGL88] Smith A., Guenther P. and Lawson R., Nucl. Phys. A483 (1988) 50.
- [SGW82] Smith A., Guenther P. and Whalen J., Argonne National Laboratory Report ANL/NDM-75 (1982).
- [SGW84] Smith A., Guenther P. and Whalen J., Nucl. Phys. A115 (1984) 1.
- [SH67] Smith A. and Hayes R., Nucl. Phys. A93 (1967) 609.
- [Sha63] Shakin C., Ann. Phys. (New York) 22 (1963) 373.
- [Smi91] Smith A., Argonne National Laboratory memorandum (1991), unpublished.

- [Smi+92] Smith A. et al., Argonne National Laboratory report ANL/NDM-127 (1992); Phys. Rev. C45 (1992) 1260; Z. Phys. A306 (1982) 265; Nucl. Instru. and Methods 50 (1977) 277; and references cited therein.
- [Smi+92A] Smith A., Guenther P., Whalen J. and Chiba S., J. Phys. G18 (1992) 629.
- [Smi94] Smith A., Nucl. Phys. A576 (1994) 165.
- [Smi95] Smith A., Nucl. Phys. A589 (1995) 201.
- [Smi96] Smith A., Nucl. Phys. A605 (1996) 269.
- [Smi97] Smith A., J. Phys. G24 (1997) 637.
- [Smi97A] Smith A., Nucl. Phys. A620 (1997) 249.
- [Smi99] Smith A., Argonne National Laboratory Report ANL/NDM-142 (1999).
- [SS97] Smith A. and Schmidt D., J. Phys. G23 (1997) 197.
- [TM69] Takeuchi K. and Moldauer P., Phys. Lett. 28B (1969) 384.
- [VSM64] Vonach W., Smith A. and Moldauer P., Phys. Lett. 11 (1964) 331.
- [WG86] Walter R. and Guss P., Proc conf. on nucl data for basic and applied sci., Eds. P. Young et al., vol. 2, p. 277 (Gordon and Breach, New York, 1986)
- [WH64] Wilmore D. and Hodgson P., Nucl. Phys. 55 (1964) 673.
- [Wol51] Wolfenstein L., Phys. Rev. 82 (1951) 690.
- [WWG60] Wyatt P., Wills J. and Green A., Phys. Rev. 119 (1960) 1031.

2. Total-cross-section data subset

- [Boc+49] Bockelman C., Peterson R., Adair R. and Barschall H., Phys. Rev. 76 (1949) 277.
- [CB67] Carlson A. and Barschall H., Phys. Rev. 158 (1967) 1142.
- [CGB52] Coon J., Graves E. and Barschall H., Phys. Rev. 88 (1952) 562.
- [DDK67] Dukarevich J., Djumin A. and Kaminker D., Nucl. Phys. A92 (1967) 433.
- [FG71] Foster D. and Glasgow D., Phys. Rev. C3 (1971) 576.
- [Goo52] Goodman I., Phys. Rev. 88 (1952) 686.
- [Ken+62] Kent L., Puri S., Snowdon S. and Bucher W., Phys. Rev. 125 (1962) 331.
- [Mil+52] Miller D., Adair R., Bockelman C. and Darden S., Phys. Rev. 88 (1952) 83.
- [ND54] Nereson N. and Darden S., Phys. Rev. 94 (1954) 1678.
- [PBS60] Peterson J., Bratenahl A. and Stoering J., Phys. Rev. 120 (1960) 521; also Phys. Rev. 110 (1958) 927.
- [PW83] Poenitz W. and Whalen J., Argonne National Laboratory Report ANL/NDM-80 (1980).
- [Rag53] Ragent T., Livermore National Laboratory Report, UCRL-2337 (1953).
- [SWG84] Smith A. Guenther P. and Whalen J., Nucl. Phys. A415 (1984) 1.
- [TS68] Tabony R. and Seth K., Ann. Phys. 46 (1968) 401.

[Vin+60] Vincent L., Morgan I. and Prudhomme J., Texas Nucl. Corp. Report, WADD-tr-60-217 (1960).

3. Differential neutron scattering data subset

- [BGS66] Becker R., Guindon W. and Smith G., Nucl. Phys. 89 (1966) 154.
- [BHB66] Buccino S., Hollandsworth C. and Bevington P., Z. Phys. 196 (1966) 103.
- [CC72] Cox S. and Cox E., Argonne National Laboratory Report ANL-7935 (1972).
- [HW71] Holmqvist B. and Wiedling T., Report AE-430 (1971); also see Report AE-482 (1973).
- [Kaz+65] Ya. Kazakova L. et al., Proc. Antwerp Conf. 576 (North Holland, 1965).
- [KST64] Korzh I., Sklyar N. and Tackig I., Ukrainskii Fizichnii Zhurnal 8 (1963) 1323.
- [Pas+58] Pasechnik M. et al., Proc. Conf. on Atoms for Peace, Geneva, United Nations Press (1958).
- [Ray59] Rayburn L., Phys. Rev. 116 (1959) 116.
- [Ste65] Stelson P. et al., Nucl. Phys. 68 (1965) 97.
- [SGW84] Smith A., Guenther P. and Whalen J., Nucl. Phys. A115 (1984) 1
- [SH67] Smith A. and Hayes R., Nucl. Phys. A93 (1967) 609.
- [SBB68] Spitz L., Barnard E. and Brooks T., Nucl. Phys. A121 (1968) 655.
- [VMP66] Vincent L., Morgan I. and Prud'homme J., WADD Report WADD-TR-60 (1966) 217.
- [WB54] Walt M. and Barschall H., Phys. Rev. 93 (1954) 1062.